ACS OMEGA

http://pubs.acs.org/journal/acsodf

Review

A Review of Molecular Models for Gas Adsorption in Shale Nanopores and Experimental Characterization of Shale Properties

Yufan Zhang, Dexiang Li,* Gongming Xin, and Shaoran Ren

Cite This: *ACS Omega* 2023, 8, 13519−13538

Read Online

ACCESS | Metrics & More | Article Recommendations

ABSTRACT: Shale gas, as a promising alternative energy source, has received considerable attention because of its broad resource base and wide distribution. The establishment of shale models that can accurately describe the composition and structure of shale is essential to perform molecular simulations of gas adsorption in shale reservoirs. This Review provides an overview of shale models, which include organic matter models, inorganic mineral models, and composite shale models. Molecular simulations of gas adsorption performed on these models are also reviewed to provide a more comprehensive understanding of the behaviors and mechanisms of gas adsorption on shales. To accurately understand the gas adsorption behaviors in shale reservoirs, it is necessary to be aware of the pore structure characteristics of shale reservoirs. Thus, we also present experimental studies on shale microstructure analysis, including direct imaging methods and indirect measurements. The advantages, disadvantages, and applications of these methods are also well summarized. This Review is useful for understanding molecular models of gas adsorption in shales and provides guidance for selecting experimental characterization of shale structure and composition.

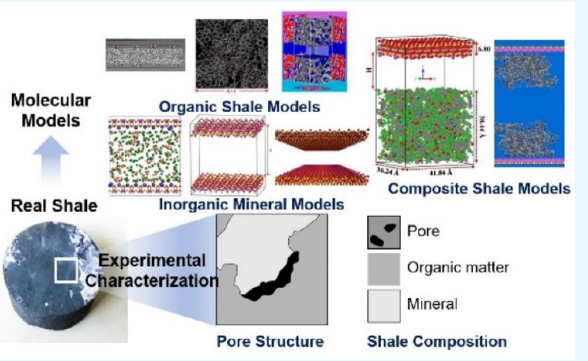

1. INTRODUCTION

Shale gas is an unconventional natural gas that has attracted much attention because of its broad resource base and wide distribution.[1] As a typical unconventional gas reservoir, shale gas reservoir has the characteristics of a large occupied area, low permeability, and low porosity.[2] Since the pore size in shale gas reservoirs is 1 order of magnitude smaller (nanoscale) than in conventional reservoirs (micron-scale), nanopores in shale gas reservoirs are crucial for the storage of shale gas.[3−5] Shale gas exists in the reservoir mainly as an adsorption state in nanopores, accounting for about 20−85% of the shale gas content.[6] Therefore, understanding the behaviors and mechanisms of adsorbed gases in nanopores is crucial to the estimation and evaluation of shale gas reserves. However, there is a great challenge for the extraction of shale gas reservoirs because the adsorption behaviors and mechanisms of shale gas in nanoporous media are still unclear.

Many breakthroughs have been made in the study of gas adsorption in shale reservoirs at the nanoscale, most of which have used molecular simulation methods. The adsorption mechanisms could not be determined directly at the molecular level by experiments.[7,8] Molecular simulations, such as grand canonical Monte Carlo (GCMC) methods, molecular dynamics simulation (MD), and density functional theory (DFT), provide feasible methods for understanding the adsorption behaviors and mechanisms of gases within nanopores with the advantage of its own calculation scale.[9] GCMC simulations create gas adsorption processes, utilizing the Metropolis sampling method by adopting the exchange, conformer, rotate, and translate processes.[10,11] MD simulations based on Newtonian mechanics are available for evaluating properties such as the position and momenta of molecules, which can achieve dynamic and thermodynamic properties with a high level of accuracy.[12] Besides, DFT simulations can provide a quantitative description of interactions between adsorbent and adsorbate.[13] Shale modeling is the basis for accurate adsorption simulations. Since shale contains a complex composition of organic matter and inorganic minerals, molecular models of different compositions have been constructed. The behaviors and mechanisms of gas adsorption differ in diverse molecular models of shale. Different shale models, including organic matter, inorganic minerals, and composite models, are presented, and molecular simulations of gas adsorption on them are described in Section 2.

In order to understand the gas adsorption behaviors in shale, it is essential to be aware of the complex pore structure

Received: February 15, 2023
Accepted: March 27, 2023
Published: April 3, 2023

https://doi.org/10.1021/acsomega.3c01036
ACS Omega 2023, 8, 13519−13538

Table 1. Recent Reviews on Shale Gas Research

number	main content	publication time	ref
1	The two-component gas transport and competitive adsorption models in the CO_2-EGR process are reviewed.	2019	Guo et al.[18]
2	The pure gas adsorption mechanism, adsorption model, and displacing properties in shale are described, and the competitive adsorption mechanism is summarized.	2020	Liu et al.[19]
3	The commonly used shale gas adsorption models are summarized in detail, and their advantages and disadvantages are pointed out.	2022	Liang et al.[20]
4	The adsorption mechanism in shale and the basic influencing factors of gas adsorption in shale are discussed.	2019	Rani et al.[21]
5	An overview of recent advances in molecular simulation studies of gas adsorption, desorption, and diffusion in the shale matrix models is presented.	2019	Wang et al.[22]
6	The effects of five submodels of the Langmuir parameters on gas adsorption capacity are examined, and the relationship between the Langmuir parameters and gas adsorption dominating factors is reviewed.	2022	Memon et al.[23]
7	A comprehensive review of shale inorganic mineral models, organic matter models, and composite shale molecular models and shale gas adsorption is presented	2021	Wang et al.[24]
8	Experimental studies on CH_4 and CO_2 adsorption in shales are reviewed, and the relationship between gas adsorption and shale properties is discussed.	2020	Klewiah et al.[25]
9	Based on in situ pilot tests, experiments, and simulation studies, the feasibility and effectiveness of gas injection methods for shale oil/gas/condensate reservoirs are discussed.	2019	Du et al.[26]
10	The results of the adsorption experiments of CO_2, CH_4, and their mixtures on coal and shale are summarized, and the effects of coal and shale properties on the adsorption are discussed.	2023	Jeong et al.[27]

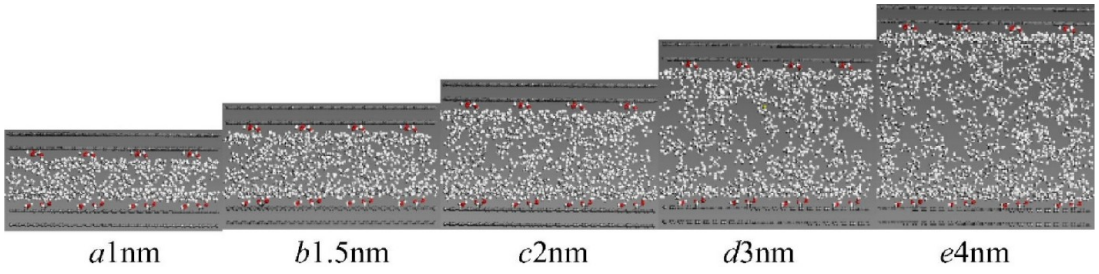

Figure 1. Snapshots of configurations of methane molecules in a multilayer graphene slit under different pore sizes. Reprinted from ref 39, Copyright 2017, with permission from Elsevier, 10.1016/j.fuel.2017.03.083.

characteristics of shale. Since the nanopore system controls the occurrence, enrichment, and aggregation of shale gas, experimental characterization of the shale microstructure is necessary to obtain the realistic pore structure of real shales, which is important for gas reservoir resource evaluation and shale gas exploration.[14−16] To clarify the complex pore system of shales, researchers have used direct imaging methods and indirect measurement techniques to characterize shale pores.[14,17] These two common types of characterization techniques are presented in Section 3, and the advantages, disadvantages, and applications of each technique are also listed therein.

Recent reviews on shale gas research are listed in Table 1, and it can be seen that there are few comprehensive reviews that combine simulation and experiments. Therefore, this Review focuses on giving a more complete reference process for shale gas research, including both molecular simulations and experimental studies. This Review provides an overview of shale models and gas adsorption simulations performed on them. Moreover, experimental studies on shale microstructure analysis are described, as a complement and correction to simulation. The present Review will provide a fundamental understanding of the molecular models for studying gas adsorption in shales and certain guidance for the choice of experimental characterization for shale structure and composition.

2. MOLECULAR MODELS OF SHALE

The composition of shale is quite complex, generally containing 30−50% clay minerals (illite, smectite, montmorillonite, etc.), 15−25% clastic minerals (quartz, calcite, carbonates, etc.), and 4−30% organic matter.[28] Besides, natural and hydraulic fractures exist in the shale reservoir, forming multiscale pore systems and different gas transport mechanisms in shale.[29,24] Kerogen is the most widely distributed and abundant group of sedimentary organic matter in shale, which strongly associates with shale gas production.[30] The composition and structure of kerogen are still not completely accurate, and thus it is represented by different molecular models which perform a few characteristics of the real kerogen to some extent.[24,31] What's more, inorganic matter accounts for a large percentage of the shale composition, the role of which thus cannot be ignored.[32] Therefore, this section will focus on different molecular models of shale construction and gas adsorption simulations performed on them.

2.1. Organic Shale Models. Organic shale models have evolved over the years from simplified shale organic models (graphene, CNTs, nanoporous materials, etc.) to realistic kerogen models. Based on these different simulation methods, various different shale organic molecular models were constructed. In this section the different shale organic models are described in detail, and the simulation results on the models are analyzed.

https://doi.org/10.1021/acsomega.3c01036
ACS Omega 2023, 8, 13519−13538

2.1.1. Multilayer Graphene Slit. To simplify the organic matter in shale and to extract the fundamental properties, two vacancy defect models were developed on the basis of graphite to obtain one-atom-thick layers of sp^2-bonded carbon, which is called graphene, with an intrinsic two-dimensional (2D) structure containing honeycomb-like carbon atoms.[33] The multilayer graphene slit is a classical simplified shale organic matter model on which a variety of simulation studies related to shale gas have been carried out.[34−36]

Cao et al. set up a multilayer graphene slit model with different distances to simulate nanopore slits, thereby predicting the CH_4 density in nanopore slits of different sizes and comparing it with bulk CH_4 density.[37] When the pore size was less than 2.0 nm, CH_4 molecules were affected by the adsorption from graphene slits. The predicted CH_4 density in nanopores deviated from the bulk density in the pore size range of 2−20 nm, which is consistent with previous molecular simulation results, as shown in Figure 1.[35,38,39] The adsorption isotherms for the total gas content and bulk and excess adsorption of methane on graphitic surfaces were calculated by molecular simulation.[35,39] It was found that the overall trend in pore size is that smaller pores exhibit higher excess density than larger ones, as shown in Figure 2.[35] The methane

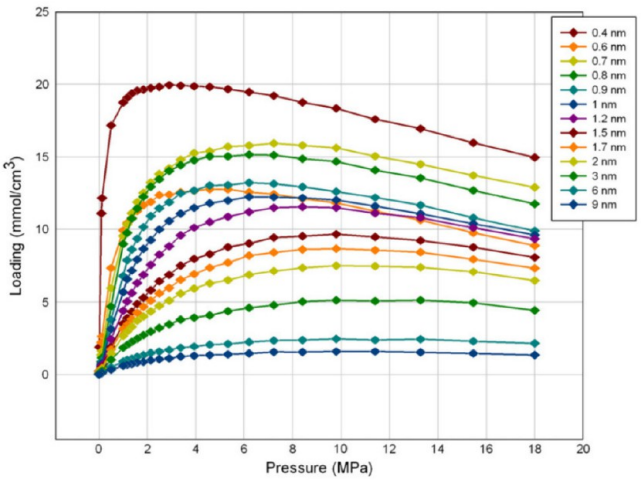

Figure 2. Excess adsorption isotherms of methane at 298 K in slit pores with pore sizes ranging from 0.4 to 9 nm. Reprinted from ref 35, Copyright 2013, with permission from Elsevier, 10.1016/j.coal.2013.01.001.

adsorption capacity increases with decreasing temperature and increasing pressure at the same pore size. Graphite layers were also used to describe the microscopic details of shale gas occurrence behavior in organic-rich nanoslits from the perspective of molecular interactions.[40] Li et al. discovered that high pressure is more favorable for gases within the nanoslit to be extracted from the wall shackles, since increased pressure leads to a significant increase in the ability to get rid of wall restraints.[40] The adsorption of methane on multilayer graphene slits can be simulated by the GCMC and MD methods, and the microscopic characterization was performed by the DFT method.[41]

In addition to the molecular simulations associated with methane, molecular simulations which are related to the CO_2 enhanced gas recovery (CO_2-EGR) project were also performed on multilayer graphene slits. Liu et al. investigated the adsorption and dynamics properties of pure CO_2, pure CH_4, and their mixtures confined in graphene slits at different temperatures and molar ratios, which is shown in Figure 3.[42] It was found that the preferential adsorption of CO_2 on the surface reduces the activation energy for CH_4 diffusion, thus improving CH_4 mobility, which has proved the feasibility of the CO_2-EGR project. Shi et al. studied the effect of the wettability of shale on CO_2 enhanced gas recovery in shale reservoirs.[43] The adsorption capacity of the graphene surface for CO_2 is stronger than that of CH_4 on a wettability model, which has a guiding value for the exploitation of shale gas. Besides, shale gas contains other hydrocarbons in addition to methane. Therefore, the injection of a mixture of shale gases (CH_4, C_2H_6, and C_3H_8) in a graphene slit model was studied.[44] The results showed that the order of selective propane > ethane > methane in the gas mixture is consistent with the same order of graphite−gas interactions. Overall, a multilayer graphene slit model can partially represent the properties of shale organic matter.

2.1.2. Carbon Nanotubes (CNTs). Carbon nanotubes, as a widely used adsorbent, are made up of a hexagonal grid of carbon atoms, which are similar to shale nanopores.[45] GCMC and MD simulations can be performed on carbon nanotubes to predict the adsorption behavior of confined gases.[46−48] Specifically, the hydrocarbon gas adsorption capacity on CNTs is stronger than that of activated carbon and graphene, which may be related to higher specific surface area and stronger interaction between adsorbent and adsorbent.[49]

The behaviors and mechanisms of methane adsorption in carbon nanopores were studied by GCMC simulations in previous studies.[50,51] Carbon nanotubes of all diameters could adsorb more methane than the bulk phase at the same temperature and pressure, and there exists an optimal carbon nanotube diameter that maximizes methane adsorption. As a result of increasing diameter of carbon nanotubes, the adsorption structure shifts from a single-file chain to two adsorption layers, which is attributed to increasing pressure exerted by the CNT wall on the adsorbed phase.[52] Besides, methane adsorption in carbon nanotubes is physisorption because isosteric adsorption heat of it is in the range of the physical adsorption.[50] As the temperature increases, the kinetic energy of methane molecules becomes larger, leading to the intensification of Brownian motion. At this time, methane molecules tend to break through the adsorption energy barrier on the surface of carbon nanotubes and change from the adsorbed state to the free state, resulting in the reduction of methane adsorption capacity.[50] In addition, the methane adsorption on triangular arrays of single-walled carbon nanotubes[53] and single-walled carbon nanohorns[52] was investigated by the GCMC method. It was found that the arrangement and diameter size of carbon nanotubes also have a large effect on methane adsorption.

MD simulations are commonly used to study the shale gas displacement in the CNT sandwiched by two tanks, as shown in Figure 4.[54,55] Yuan et al. set up the adsorption model on which CH_4 molecules were preadsorbed on the CNT wall first.[55] The displacement of preadsorbed CH_4 in CNTs by CO_2 injection was explored on the model, and the CNT was fixed during the whole process and connected with the bulk phase of CH_4. The results showed that there exists an optimal carbon nanotube diameter for the CO_2-injected displacement of CH_4, allowing the highest CH_4 recovery efficiency. Injection of CO_2 into the CNT can increase the recovery of CH_4 by at least 14.78% over that achieved through pressure drawdown.[55]

https://doi.org/10.1021/acsomega.3c01036
ACS Omega 2023, 8, 13519−13538

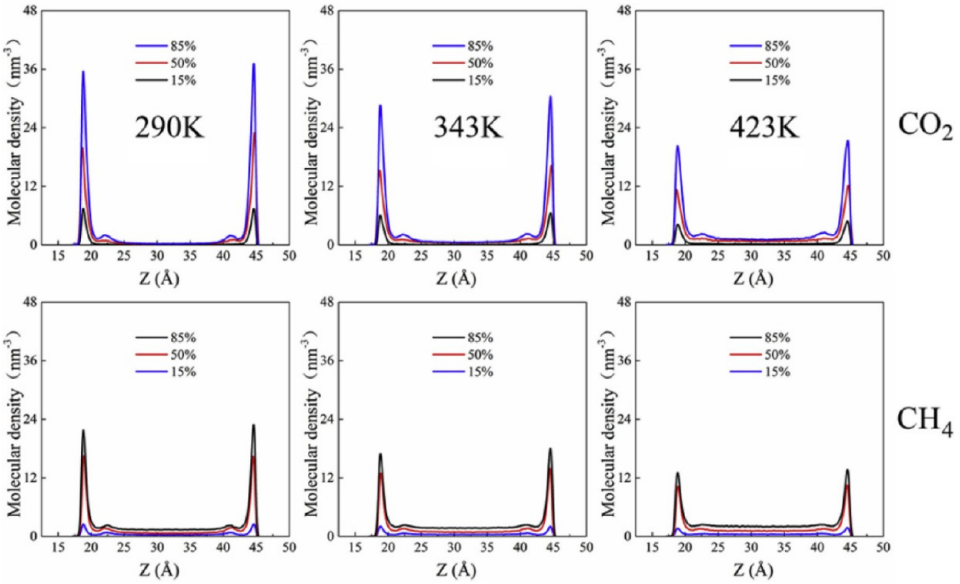

Figure 3. Two-component density profiles of three temperatures at 290, 343, and 423 K. Molecular density profiles for CO_2 (top) and CH_4 (bottom) in mixtures of a total of 600 molecules. The CO_2:CH_4 ratios of mixtures are at 15:85, 50:50, and 85:15 with black, red, and blue lines, respectively. Reprinted from ref 42, Copyright 2018, with permission from Elsevier, 10.1016/j.jngse.2018.02.034.

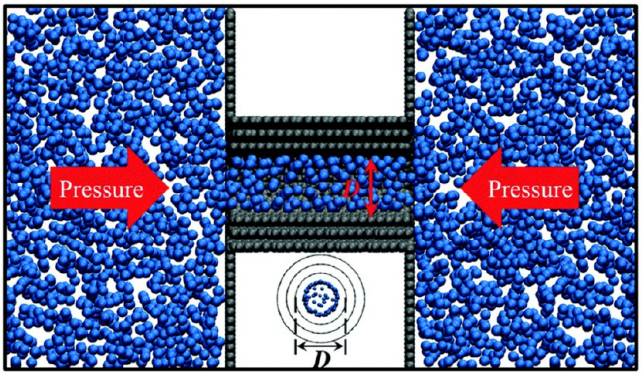

Figure 4. Adsorption model of MD simulations. The blue and gray balls represent CH_4 molecules and carbon atoms, respectively. Republished with permission of the Royal Society of Chemistry, from ref 55, Copyright 2015; permission conveyed through Copyright Clearance Center, Inc.

The self-diffusion coefficient of methane in the interior of constricted CNTs models was calculated using the MD simulations.[56] The calculated diffusion coefficient declined with increasing carbon nanotube diameter.

2.1.3. Nanoporous Carbons (NPCs) with Functional Groups. Since real shale organic matter contains a large number of functional groups, functional groups including hydroxyl (−OH), carboxyl (−COOH), epoxy (−OX), carbonyl (−CO), and nitrile (−CN) were introduced into the nanoporous carbons model to obtain a reasonable model that is more closely matched with real shale.[57−59]

The adsorption behavior of methane on nanoporous carbon containing different functional groups varies widely. Among them, the models containing hydrophobic groups have a greater adsorption capacity than that containing hydrophilic groups.[60] Furthermore, competitive adsorption of a binary CO_2−CH_4 mixture in nanoporous carbons was studied for the CO_2-EGR project.[57,59] Zhang et al. found that the selectivity of CO_2/CH_4 in the nanoporous carbon model containing functional groups was higher than that in the nanoporous carbon model without functional groups.[59] The results showed that the selectivity of CO_2/CH_4 in nanoporous carbon containing different functional groups was in the order of epoxy > carbonyl > carboxyl > hydroxyl > nitrile, as shown in Figure 5.[59] Lu et al. discovered that the effect of functional groups on CO_2 adsorption was greater than that on CH_4 adsorption, so that the selectivity of CO_2 over CH_4 was significantly higher at low pressure, in the order of NH_2−NPC > COOH−NPC > OH−NPC > H−NPC > NPC.[57] Overall, the introduction of functional groups has undoubtedly further reduced the variation between molecular models and real shale organic matter, and thus the simulations performed on nanoporous carbon containing functional groups are more informative.

2.1.4. Kerogen Model. The shale organic matter is mainly composed of kerogen, which is considered to be the dominant methane trap. Kerogen is sedimentary organic matter insoluble in common polar solvents, such as chloroform and dichloromethane.[61] The physicochemical properties of kerogen depend on the origin and on the burial history.[62] Kerogen can be classified into three different types:[63] (i) type I from a lacustrine anoxic environment, (ii) type II from marine shales and continental plankton, and (iii) type III from plants in tertiary and quaternary coals. The entire process is shown in Figure 6.[63] Since the elemental and functional group data of different types of kerogen have been reported in the previous work, kerogen models with similar structure and properties to real shale organic matter are also gradually established.[61,63] The dynamic and thermodynamic properties of gas molecules can be better predicted in these kerogen models because they are able to simulate a more realistic structure of shale.[7] What's more, kerogen models can provide experimental environments for gas adsorption research under the real shale reservoir conditions, allowing for a better understanding of the mechanisms of gas adsorption at a microscopic level. In this section, the latest advances in kerogen models and relative simulations are introduced.

https://doi.org/10.1021/acsomega.3c01036
ACS Omega 2023, 8, 13519−13538

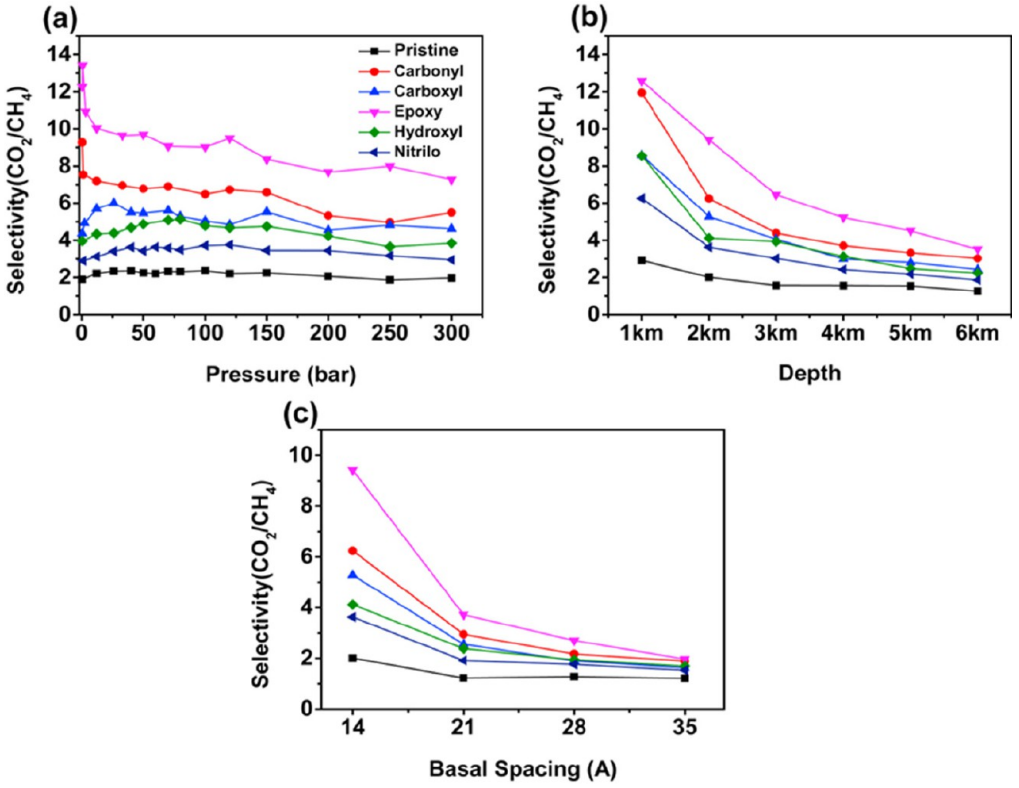

Figure 5. (a) Selectivity of CO_2/CH_4 in the organic-rich shale model and pristine pillared shales model at T = 370 K. (b) Selectivity of CO_2/CH_4 at different depths. (c) Selectivity of CO_2/CH_4 at different basal spacings. The bulk CO_2 mole faction of y_{CO_2} = 0.5. Reprinted from ref 59, Copyright 2017, with permission from Elsevier, 10.1016/j.jngse.2017.01.024.

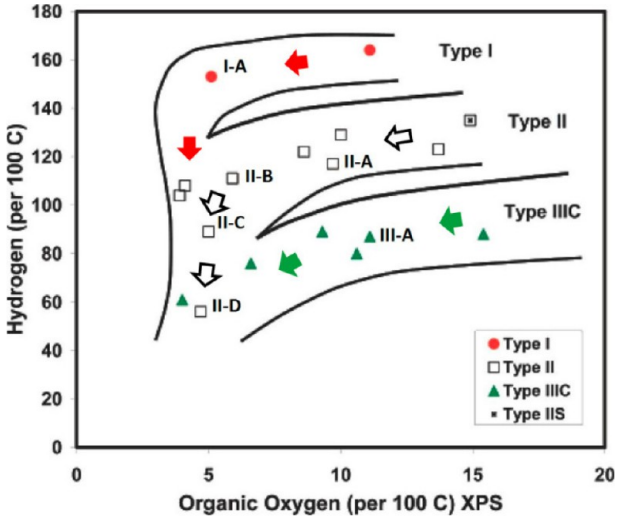

Figure 6. Van Krevelen diagram for kerogen using hydrogen from elemental analysis and organic oxygen from XPS analysis. Reproduced from ref 63, Copyright 2007, American Chemical Society.

In order to reveal the complex nanoscale structure and properties of kerogen, Kelemen et al. obtained elemental and functional group data of kerogen based on the analysis of real shales, which prepared for the subsequent modeling of kerogen.[63] Ungerer et al. developed molecular models of casein at different maturity levels on the basis of the above data, which to some extent reproduced the kerogen in real shales, and these models were widely used in the later simulation work.[61,64−71] The simulation results of these different types of kerogen models matched with experimental data with reasonable accuracy.[64,69,72] Thus, this method of constructing kerogen models proposed by Ungerer et al. also offers the possibility of understanding kerogen structures and developing better molecular kerogen models.

Several molecular simulations of gas adsorption behaviors in shale were carried out using kerogen matrix models.[62,64,66,72,73] The process of constructing the kerogen matrix model is shown in Figure 7.[69] Both adsorption on the surface of the kerogen matrix and adsorption within it result in a high adsorption capacity. Previous studies have shown that the affinity and adsorption capacity of CO_2 on the kerogen matrix are higher than those of CH_4, providing strong evidence for the feasibility of CO_2-EGR projects.[68,69,73,74] In addition, real shale reservoirs often contain a certain amount of water; therefore, research on the moist kerogen matrix is also necessary. Chong et al. investigated the adsorption of carbon dioxide, methane, and water in the immature type II-A kerogen matrix model, using MD and GCMC simulations.[64] The adsorption isotherms showed that the adsorption capacities of methane and carbon dioxide on the kerogen matrix were similar (up to 1.5 mmol/g) and both less than that of water (up to 6.2 mmol/g), which was due to the strong water−kerogen energy interactions and the tendency to form large water clusters. Furthermore, the pore volume of the kerogen matrix is influenced by the presence of water molecules.[72] The enterable pore volume decreased with increasing water content, leading to a decrease in the adsorption of CH_4 and CO_2.[64,72] The maturity of kerogen also has an effect on gas adsorption, and in general, there is a positive correlation between the gas adsorption capacity on the matrix and the maturity of

https://doi.org/10.1021/acsomega.3c01036
ACS Omega 2023, 8, 13519−13538

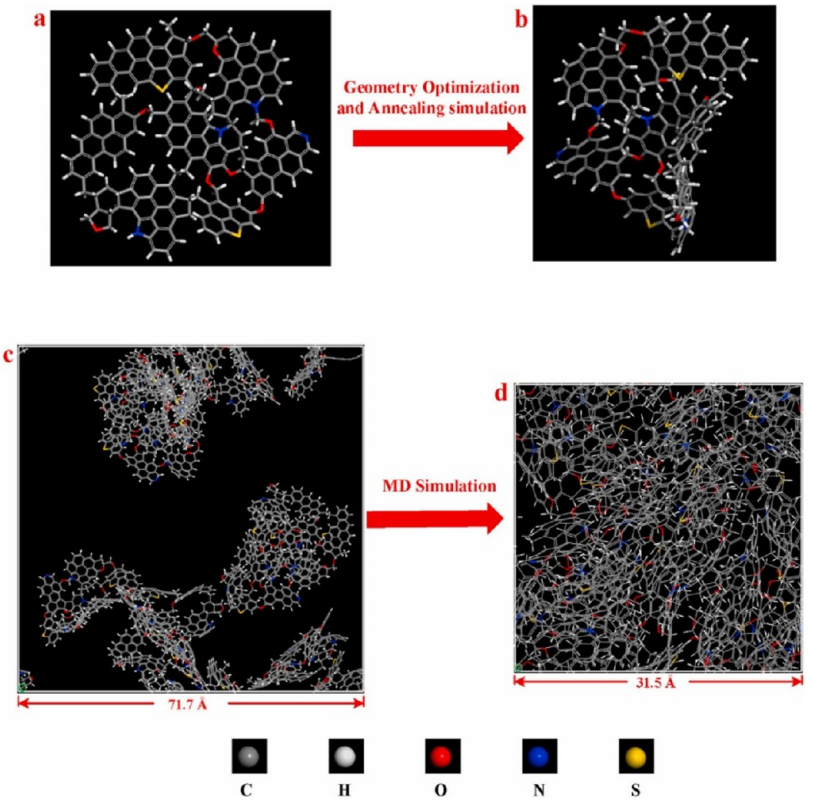

Figure 7. (a) Initial structure of the kerogen II-D unit; (b) structure of the kerogen II-D unit after the geometry optimization and annealing dynamics; (c) initial kerogen model configuration; (d) final kerogen model configuration. Atoms: C in gray, H in white, O in red, N in blue, and S in yellow. Reprinted from ref 69, Copyright 2021, with permission from Elsevier, 10.1016/j.jngse.2021.103903.

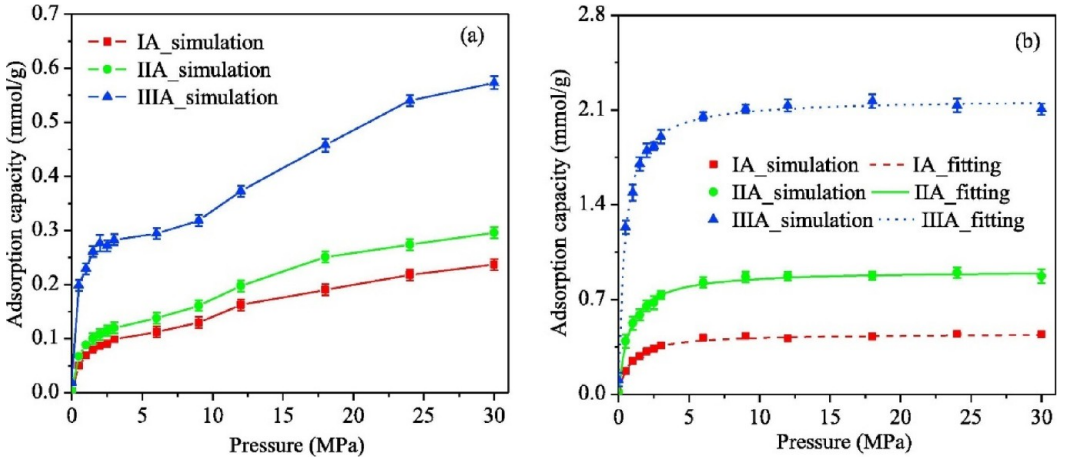

Figure 8. Absolute adsorption isotherms of CH_4 and CO_2 in the binary mixtures on dry kerogen models of different organic types at 338 K with y_{CO_2} = 0.5. (a) CH_4 absolute adsorption isotherms; (b) CO_2 absolute adsorption isotherms. Reprinted from ref 72, Copyright 2017, with permission from Elsevier, 10.1016/j.apenergy.2017.10.122.

kerogen.[72,75] The competitive adsorption behaviors of CH_4 and CO_2 on the kerogen matrix models of different organic types were investigated, as shown in Figure 8.[72] It was found that the CO_2 and CH_4 adsorption capacity and adsorption selectivity were in the order of kerogen I-A < II-A < III-A, which was consistent with the sequence of enterable pore volume fraction.[72] Meanwhile, the kerogen matrix is a dynamic system, and a coupling may exist between gas adsorption and kerogen matrix structure deformation.[73] Pathak et al. found that methane and carbon dioxide adsorption on the kerogen matrix could swell the kerogen matrix.[66] What's more, the CO_2 adsorption swelled the kerogen matrix to a smaller order of magnitude than that caused by adsorption of equal moles of methane, which is beneficial for CO_2 sequestration in shale reservoirs.[66] This means that if the CO_2 injected into the shale formation is roughly equal to or less than the gas-in-place (GIP), the volume of the kerogen matrix may shrink rather than swell. Moreover, the radial distribution function (RDF) describes the density as a function of distance from the reference particle and is an essential tool to study the structural information on gas adsorption in the kerogen matrix.[62] Sui and Yao found that the N- and S-containing functional groups in

https://doi.org/10.1021/acsomega.3c01036
ACS Omega 2023, 8, 13519−13538

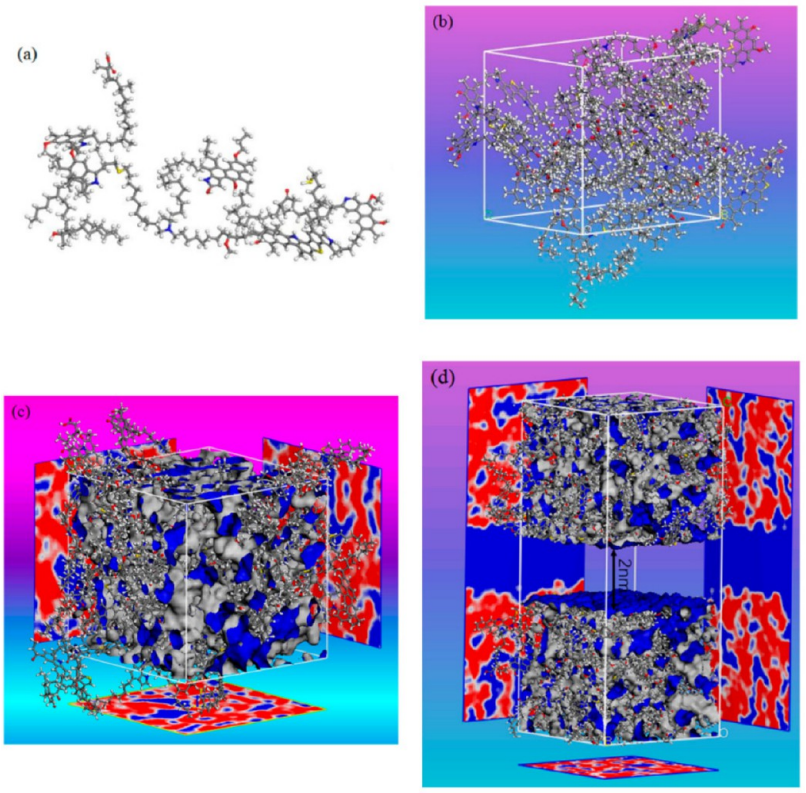

Figure 9. (a) Molecular model of a type I-A kerogen molecule with the chemical formula $C_{251}H_{385}O_{13}N_7S_3$; (b) bulk kerogen configuration with 10 kerogen molecules; (c) bulk kerogen model with porosity; (d) structure of a realistic slit kerogen nanopore. Reproduced from ref 79, Copyright 2020, Multidisciplinary Digital Publishing Institute.

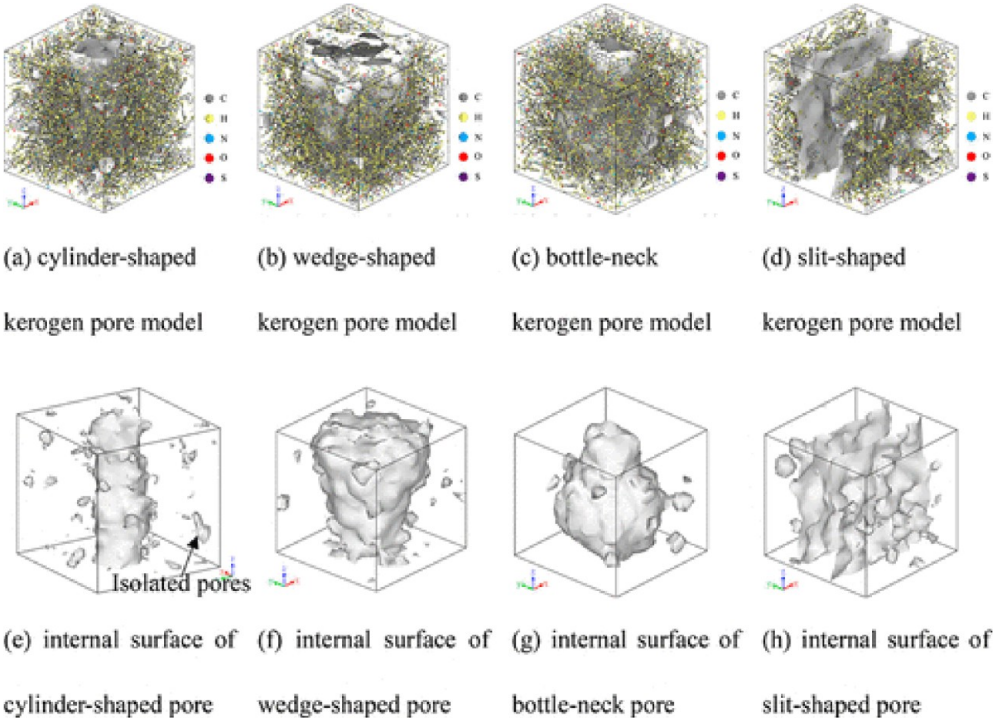

Figure 10. Visualization of constructed kerogen pore structures and corresponding internal surfaces/isolated pore surfaces. Reproduced from ref 78, Copyright 2020, American Chemical Society.

kerogen have a positive effect on CH_4 and CO_2 adsorption, inferring that CH_4/CO_2 is preferentially adsorbed on the N/S-containing functional groups of the kerogen matrix.[62]

Although the kerogen matrix models with pores are capable of representing shale organic matter, the presence of natural fractures in the real shale reservoirs results in a wider range of

https://doi.org/10.1021/acsomega.3c01036
ACS Omega 2023, 8, 13519−13538

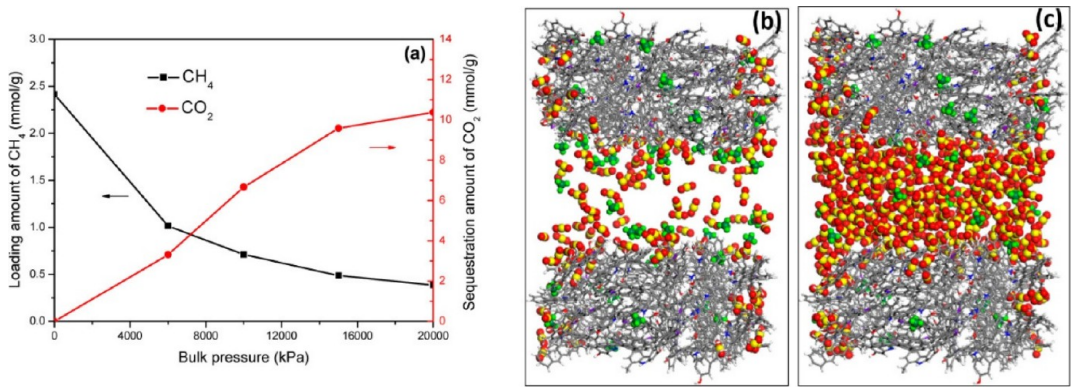

Figure 11. (a) Loading amount of CH_4 (black line) and sequestration amount of CO_2 (red line) with the variation of bulk pressures in kerogen slit nanopores at 323 K, with the corresponding snapshots of the residual gases in kerogen slit nanopores at the bulk pressure of 6 (b) and 20 (c) MPa. Reproduced from ref 69, Copyright 2017, American Chemical Society.

pore size system than the kerogen matrix model. Only micropores and no mesopores are observed in the kerogen matrix model, leading to pore size system limitations in the model, which result in a limiting gas adsorption capacity.[76] Research related to shale organic matter requires models with multiscale structures. Therefore, the kerogen slit model satisfying multiscale structures is generated, which can be constructed in two ways: one is to form slit pores using two blocks of matrix models, and the other is to dummy particles or cutter atoms in the kerogen model, which are shown in Figures 9 and 10, respectively.[70,71,77−79]

The competing adsorption behaviors of CO_2 and CH_4 in kerogen slit nanopores were investigated and compared with the kerogen matrix.[69] The adsorption capacity of CH_4 and CO_2 in the kerogen slit nanopores is greater than that in the kerogen matrix at the same temperature and pressure. However, the adsorption selectivity of CO_2 over CH_4 in the kerogen matrix is greater than that in the kerogen slit nanopores.[69] This means that more CH_4 can be displaced from a shale reservoir without slits (or fractures) when the same amount of CO_2 is injected. Sun et al. investigated a displacement process of the residual adsorbed CH_4 by CO_2 in kerogen slit nanopores and found that with the increase of the bulk pressure, the displacement efficiency increased and the CO_2 sequestration amount in the slit nanopores of kerogen rose at the same time, which is shown in Figure 11.[69] Moreover, confinement effects were observed in both micropores and small mesopores of the kerogen slit model, which resulted in part of the CH_4 being firmly adsorbed in the intrinsic pores of the kerogen matrix, making it difficult for CO_2 injection to displace it.[69,71] Recently, the competitive adsorption between CO_2 and typical hydrocarbon components (CH_4, C_2H_6, and C_3H_8) in the kerogen slit was also studied.[70] It was found that according to the competitive adsorption behaviors for hydrocarbon mixtures, CO_2 huff-n-puff is more favorable for recovery of heavier hydrocarbons, while pressure drop is suitable for production of lighter hydrocarbons. Furthermore, the pore structures of the real shale are very complex, and the main pore structures can be classified into four types based on experiments: cylinder-shaped pores, bottleneck pores, wedge-shaped pores, and slit-shaped pores.[80,81] Liu et al. found that pore structure had a significant effect on shale gas recovery, and the difficulty for CH_4 molecules to be displaced in different pore structures was in the order of cylinder-shaped > bottleneck > slit-shaped > wedge-shaped pores.[78]

2.2. Inorganic Mineral Models. Inorganic minerals account for the main body of shale, which always have important effects on the reserve and transport properties of gases in shale. Among the shale clay minerals, the main components are illite, montmorillonite, and kaolinite.[82] In addition, quartz is a major component of the mineralogical composition of shale.[82] In recent years, there has been an increasing number of studies focusing on the structure and properties of shale inorganic minerals and using molecular simulations to study the gas adsorption behaviors in inorganic minerals.[83−87] Therefore, two main shale inorganic mineral models are presented in this section: one is the clay mineral model, which consists of aluminum phyllosilicates, and the other is a quartz nanopore composed of silicon and oxygen atoms.

2.2.1. Clay Mineral Models. Montmorillonite is a clay mineral widely distributed in some shale formations; for example, clay-dominated shale samples from Sichuan, China contain up to 78.7% montmorillonite.[88] The common Na-montmorillonite mineral model was a Wyoming-type, with a three-layer structure including two tetrahedral (Si−O) layers and an octahedral (Al−O) layer.[89] Sun et al. investigated the adsorption properties of CH_4 and CO_2 in montmorillonite slit-nanopores and found that the positively charged Na^+ ions on the surface of montmorillonite have a positive effect on the CO_2 adsorption.[90] This is because the O atoms in CO_2 molecules can be attracted to Na^+ ions on the surface, while H atoms in CH_4 molecules repel them. Besides, at a fixed CO_2 injection pressure, the displacement amount of CH_4, the percentage of displacement, and the sequestration amount of CO_2 in the montmorillonite slit model all decrease significantly with decreasing pore size and increasing geological depth.[91] Adsorption studies on hydrocarbon mixtures were also performed in montmorillonite slit-nanopores, as shown in Figure 12, and it was found that the adsorption selectivity of C_2H_6 over CH_4 decreased monotonically with increasing pressure, which is shown in Figure 13, indicating preferential adsorption of C_2H_6 molecules at low pressure and a higher adsorption of CH_4 molecules at high pressure.[92] Stronger interactions between C_2H_6 molecules and larger molecular size are responsible for the preferential adsorption shift.[92]

Another clay mineral in shale is illite, the highest proportion of clay minerals in gas-bearing shales in China, especially in the

https://doi.org/10.1021/acsomega.3c01036
ACS Omega 2023, 8, 13519−13538

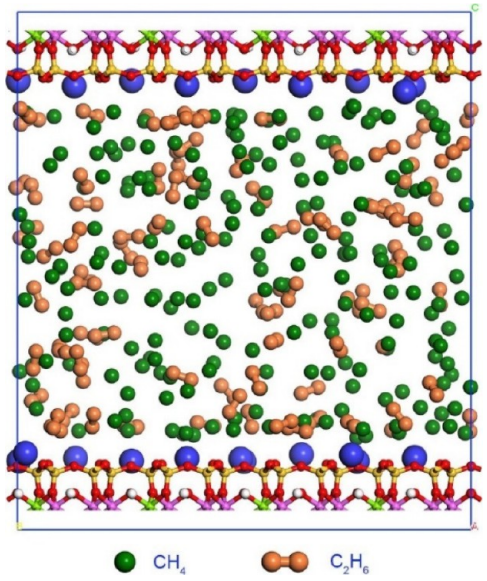

Figure 12. Schematic diagram showing competitive adsorption of a CH_4/C2H_6 mixture in a 3.0 nm MMT slit. Dark green and orange spheres represent the united-atom models of CH_4 and C_2H_6, respectively. Color scheme: pink, Al; light green, Mg; blue, Ca; red, O; yellow, Si; white, H. Reprinted from ref 92, Copyright 2019, with permission from Elsevier, 10.1016/j.cej.2018.08.067.

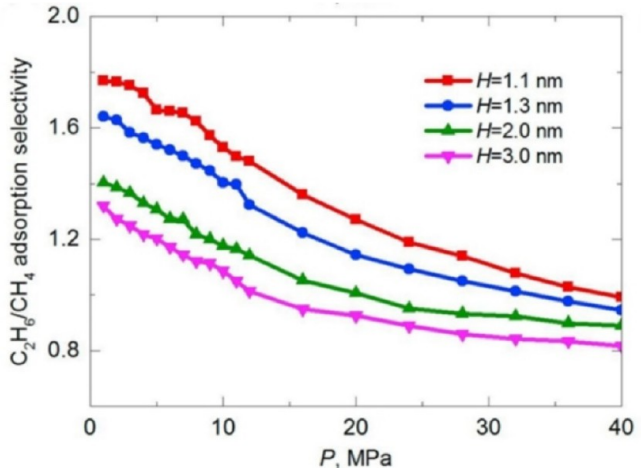

Figure 13. Selectivity of C_2H_6 relative to CH_4 versus pore pressure P ($y_{C_2H_6}$ = 0.3). Reprinted from ref 92, Copyright 2019, with permission from Elsevier, 10.1016/j.cej.2018.08.067.

Yangzi region.[93] The K-illite model is typically used in molecular simulations, which is represented by dioctahedral illite with the general unit cell formula of $K_x[Si_aAl_{8-a}][Al_bMg_{4-b}]O_{20}(OH)_4$.[94] Using the GCMC method, Chen et al. simulated the adsorption behavior of CH_4 and CO_2 in K-illite slit pores and revealed the key gas adsorption mechanism.[85,95] CH_4 molecules without polarity are adsorbed in the center of the six-membered oxygen ring on the silicon oxygen tetrahedron surface, while CO_2 molecules with an electric quadrupole moment are closer to the polar oxygen atoms in the ring, so the electric quadrupole moment makes the adsorption capacity of CO_2 in the K-illite pores much greater than that of CH_4.[95] The clay pores of shale formations are expressed as basal surfaces and edge surfaces, where in illite the edge surface is dominated by the A and C chain surface and the B chain surface.[96] Molecular models of these surfaces in illite are shown in Figure 14.[97] Hao et al. found that methane adsorption was in the order of basal surface > B chain surface > A and C chain surface, as shown in Figure 15, and the difference in adsorption capacity between these surfaces was negligible.[97] This suggests that the edge surface pores have comparable adsorption capacity to the basal surface pores, whose influence is not negligible in real shale formations.

Kaolinite is a typical type of clay mineral in shale. The kaolinite mineral model, which is shown in Figure 16, is composed of 1:1 dioctahedral layers, which consist of a sheet of corner-sharing SiO_4 tetrahedra and a sheet of edge-sharing AlO_6 octahedra.[98,99] Zhou et al. investigated the adsorption mechanism of pure CH_4 and CO_2/CH_4 mixtures in kaolinite slit pores using the GCMC method.[99] The results showed that both monolayer adsorption and micropore-filling adsorption mechanisms existed in kaolinite slit pores, and the micropore-filling adsorption tended to be significant as the pore size decreased or the pressure increased.[99] The adsorption behaviors of CH_4 in kaolinite with water contents have also been analyzed by MD and MC methods.[100,101] It was found that a higher water content would cause a weaker interaction energy between CH_4 and kaolinite.[102] This is owing to the fact that water molecules preferentially adsorb on oxygen and hydrogen atoms in kaolinite, seizing the adsorption sites of CH_4 on kaolinite.[100] Besides, due to the large amount of defective elements in kaolinite, Wang et al. investigated the effect of Mg, Fe(II), and Al doping on CH_4 adsorption on the surface of kaolinite (001).[102] The simulation results showed that all kinds of ion doping can significantly reduce the adsorption of CH_4 on kaolinite, which is because ion doping reduced the strength of the interaction between CH_4 and the kaolinite surface.[102]

Moreover, selective adsorption behaviors of CO_2/CH_4 have been investigated through diverse clay mineral types.[83,84] It was generally found that the order of adsorption selectivity of CO_2 over CH_4 on different clay minerals was kaolinite < illite < montmorillonite, as shown in Figure 17.[83] This is attributed to the fact that CO_2 molecules are more likely to adsorb on the surface of montmorillonite and illite nanopores with cation exchange than on the surface of kaolinite nanopores without cation exchange.[83,84]

2.2.2. Quartz Models. Quartz is an important part of shale reservoirs and has various forms such as α-quartz, β-quartz, coesite, and stishovite, among which α-quartz is the most stable and widely distributed in sedimentary, magmatic, and metamorphic rocks.[87] α-Quartz crystal is characterized by a hexagonal structure with the space group $P3121$.[103] The hydrophilic/hydrophobic properties of the quartz nanopore surface have a significant effect on the gas adsorption. Sun et al. investigated the adsorption behaviors of pure CH_4 and binary-mixed CH_4 and CO_2 in quartz nanopores with different hydrophilic/hydrophobic surfaces and found that the hydrophilic surface had a significant contribution to the CO_2 adsorption, while the hydrophobic surface was beneficial for the CH_4 adsorption.[104] The microscopic mechanism of CO_2 and CH_4 adsorption on α-quartz surfaces was investigated by means of DFT.[103] The simulations revealed that due to polar interactions, CO_2 molecules on quartz nanopore surfaces prefer to adsorb near hydroxyl groups, while CH_4 molecules prefer to adsorb preferentially near methyl groups.[103,104] Yang et al. found that the CO_2/CH_4 adsorption selectivity in quartz nanopores was greater than 1, which can be observed in Figure

https://doi.org/10.1021/acsomega.3c01036
ACS Omega 2023, 8, 13519−13538

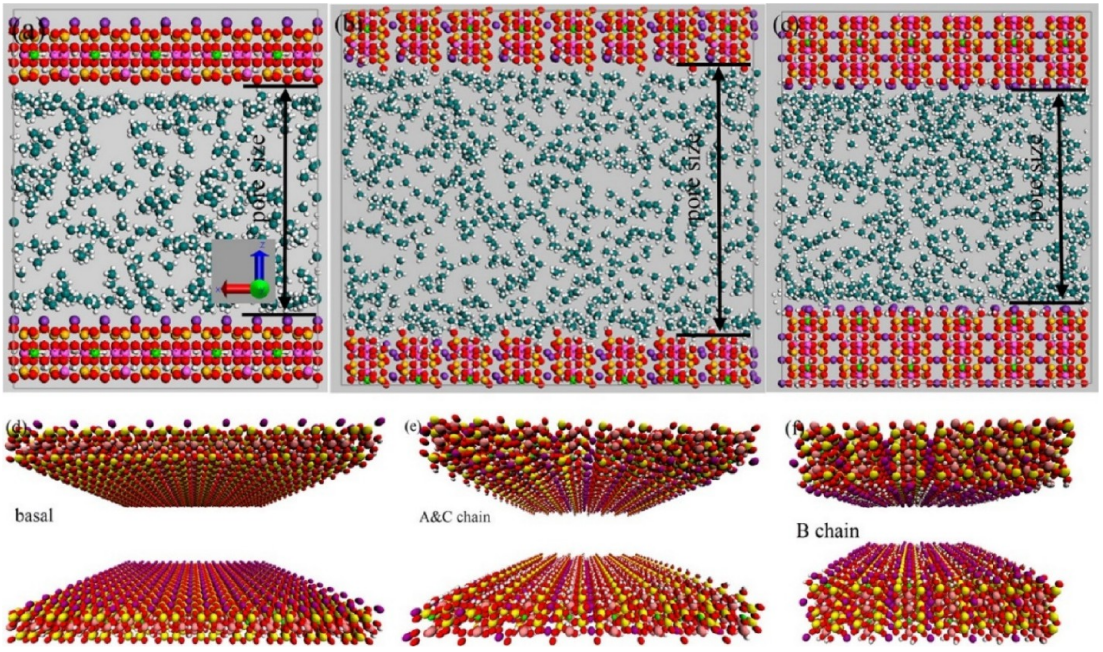

Figure 14. Illustration of a molecular model of illite (a) basal slit pore, (b) A and C chain slit pore, and (c) B chain slit pore with adsorbate CH_4 in the equilibrium state (from an orthographic view) and (d) basal slit pore, (e) A and C chain slit pore, and (f) B chain slit pore (from a perspective view). Color scheme: yellow, silicon; pink, aluminum; green, magnesium; red, oxygen; purple, potassium; cyan, carbon; white, hydrogen. Reproduced from ref 97, Copyright 2018, American Chemical Society.

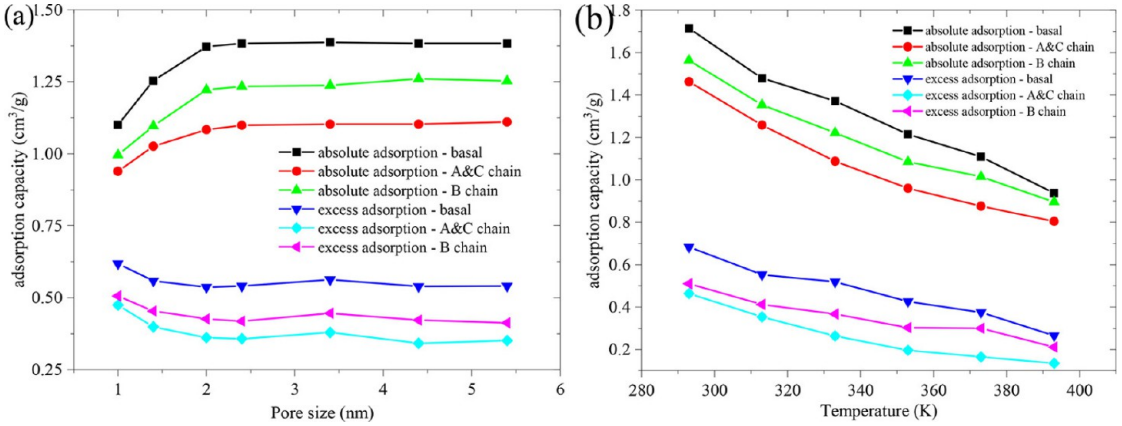

Figure 15. (a) Pore size dependence (333 K, 10 MPa) and (b) temperature dependence (3 nm pore, 10 MPa) of simulated adsorption capacity in different illite slit pores. Reproduced from ref 97, Copyright 2018, American Chemical Society.

18, indicating the adsorption advantage of CO_2 over CH_4, which illustrates the feasibility of the CO_2-EGR project.[87] The effect of water molecules on methane adsorption in quartz nanopores was also investigated, and it was found that water molecules in quartz nanopores were oriented to occupy the pore walls and take up the adsorption space of methane molecules, resulting in reduced methane adsorption capacity.

2.3. Composite Shale Models with Organic and Inorganic Matter. The two main types of geological models used in the previous research are inorganic and organic matter models, which are simple in structure and cannot accurately and graphically represent the true microscopic state in shale reservoirs. In addition, both organic matter and inorganic minerals have an influence on the adsorption behaviors of shale gas, while the overall adsorption properties of shale cannot be expressed by simply adding up the adsorption capacity of inorganic minerals and organic matter.[105,106] Thus, it is necessary to construct a composite shale model that includes inorganic minerals and organic matter to represent the real shale, which is closer in composition to the real shale and has a more comprehensive level of adsorption than the individual organic and inorganic mineral models.[91]

In the composite shale model developed by Lyu et al, as shown in Figure 19, montmorillonite was used to represent inorganic clay minerals, and kerogen was used to represent organic matter, both of which were treated as rigid materials.[107] It was found that the difference in methane adsorption between montmorillonite and kerogen was little in the smaller composite nanopores.[107] Lee et al. constructed a composite shale model containing quartz and CNTs regions, in which CNTs and quartz were hydrophobic and hydrophilic, respectively.[106] Gong et al. built a composite shale model consisting of two kaolinite layers and two kerogen II-D layers to study the displacement characteristics of CH_4 by CO_2, as

https://doi.org/10.1021/acsomega.3c01036
ACS Omega 2023, 8, 13519−13538

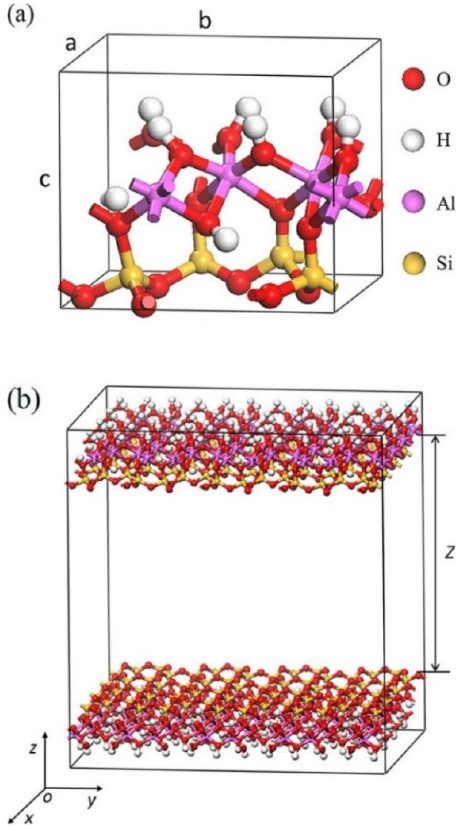

Figure 16. Molecular models: (a) kaolinite, $Si_4Al_4O_{10}(OH)_8$; (b) slit-shaped supercell kaolinite pore. Color scheme: red, oxygen; white, hydrogen; pink, aluminum; yellow, silicon. Reproduced from ref 99, Copyright 2019, American Chemical Society.

shown in Figure 20.[108] It was found that the increase of formation temperature and pore size could improve the displacement efficiency of CH_4. An accurate description of shale composition and structure is critical to the molecular simulation of shale gas adsorption, so the establishment of a more accurate composite shale model is the key to future simulation research.

2.4. Model Validation. Model validation is an integral part of the simulation which ensures that the simulation work is somewhat realistic and not just a random fabrication. Several common methods exist in the validation of shale models. First, the final density of the model should be compared with the density profile of the real reservoir. For example, the simulated density of the kerogen matrix model constructed by Sun et al. is 1.17 ± 0.03 g/cm^3, close to the experimental value of 1.181 g/cm^3.[69] Second, before simulating the adsorption process, a force field validation of the adopted force field parameters is required.[109] This allows the model to be further validated by comparing simulated CH_4 adsorption isotherms with experimentally measured CH_4 adsorption in shale samples. Huang et al. compared the simulated and experimentally obtained CH_4 excess adsorption isotherms, as shown in Figure 21, finding that the uncertainty for type I and type II kerogen was negligible.[72] In contrast, the standard deviation for type III kerogen can reach 0.034 mmol/g. However, this uncertainty is acceptable as it is within ±3% for different configurations. With the help of the experimental data from real shale and sophisticated simulators, the uncertainty of the currently constructed model is within acceptable limits. There are two types of simulators currently in general use: the first is classic molecular simulation software, such as Lammps and Materials studio, which is often used as for GCMC and MD simulations, and the second is a simulator suitable for unconventional gas and oil reservoir simulation, including ECLIPSE and GEM, which are capable of predicting reservoir production dynamics.[110,111]

3. EXPERIMENTAL STUDIES ON SHALE MICROSTRUCTURE ANALYSIS

The shale is mainly composed of various micrometer- and nanometer-size pore types that are associated with organic matter and clay minerals.[112] In order to estimate the shale gas reservoir potential, it is necessary to understand the pore structure characteristics. Therefore, experimental characterization of shale samples is necessary. In previous studies, the pore network of shale rocks has been documented by quantitative and qualitative techniques.[16,113,114] However, the microstructural characterization of shale gas reservoirs remains a challenge due to ultrafine grained microfabric and microlevel heterogeneity of shale rocks.[14] The purpose of this section is to summarize some experimental methods for shale microstructure analysis. Two experimental methods to analyze the pore structure are indirect measurement and direct imaging methods, which can characterize the specific surface area and pore size distribution (PSD), pore volume, and total porosity to describe complex shale pore systems.[14,16] The range of pore sizes that can be observed with these techniques is shown in Figure 22.[14]

3.1. Direct Imaging Methods. To understand the complex nanoscale pore system of shale, direct imaging techniques such as nano-CT, scanning electron microscopy (SEM), transmission electron microscopy (TEM), and focused ion beam scanning electron microscopy (FIB-SEM) have been used to characterize shale pores.[15,113,115] According to IUPAC (International Union of Pure and Applied Chemistry), pores are divided as micropores (<2 nm), mesopores (2−50 nm), and macropores (>50 nm). Since the proportion of mesopores and micropores in shale pores is considerable, the nano-CT technique, whose maximum resolution is slightly less than 50 nm, has difficulty in meeting more accurate imaging standards and has been used less frequently in recent years.[15]

SEM is an imaging technique for direct observation of porosity in 2D images with relatively low resolution.[116] TEM can observe pore structures smaller than 2 nm and requires samples with electron transparency and X-ray transparency (thinner than 200−250 nm).[14] Both SEM and TEM are commonly applied imaging techniques in analyzing shale pore structure; SEM excels in observing mesopore structure, while TEM is more accurate in micropore observation.[14] Combination of the two imaging techniques can reflect the true pore size distribution of shale samples comprehensively and is suitable for nanoscale characterization of shale gas reservoirs.[117,118] Zhou et al. conducted a 2D characterization of shale samples from the Lower Silurian Longmaxi Formation in the southern Sichuan Basin by SEM techniques.[15] The results showed that the nanopore structure can be divided into three types: organic pores, inorganic pores, and microfractures, among which the Longmaxi Formation shales are dominated by organic pores. Another example is the Horn River Shale Reservoir in Canada, where the main structure observed by SEM and TEM imaging consists of organic matter pores, intraparticle pores, and interparticle pores.[115] An emission

https://doi.org/10.1021/acsomega.3c01036
ACS Omega 2023, 8, 13519−13538

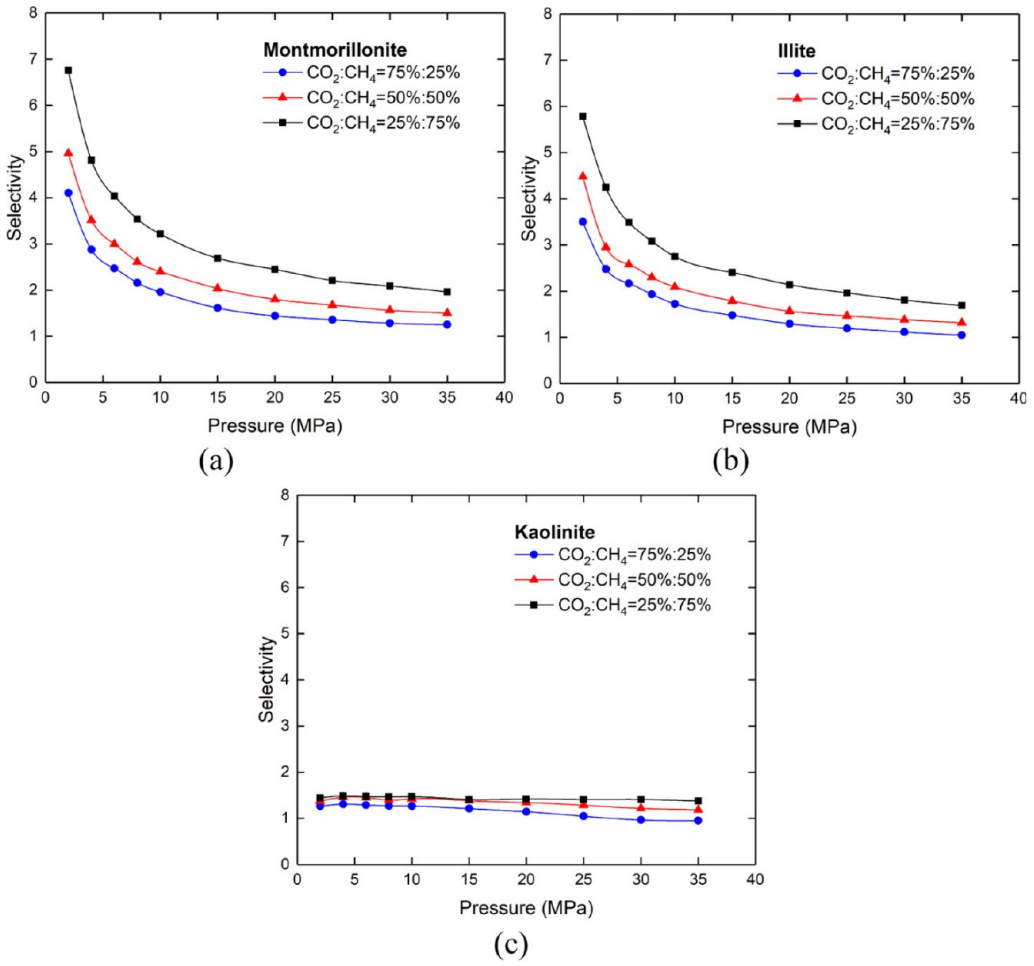

Figure 17. Selectivity for different molar fractions at T = 333.15 K in (a) montmorillonite, (b) illite, and (c) kaolinite nanopores. Reproduced from ref 83, Copyright 2019, American Chemical Society.

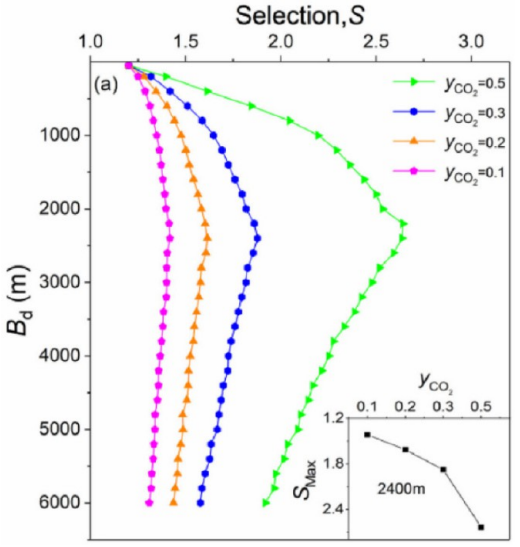

Figure 18. Selectivity of CO_2/CH_4, S, at varied y_{CO_2} in anhydrous quartz nanoslit. Reprinted from ref 87, Copyright 2022, with permission from Elsevier, 10.1016/j.energy.2021.122789.

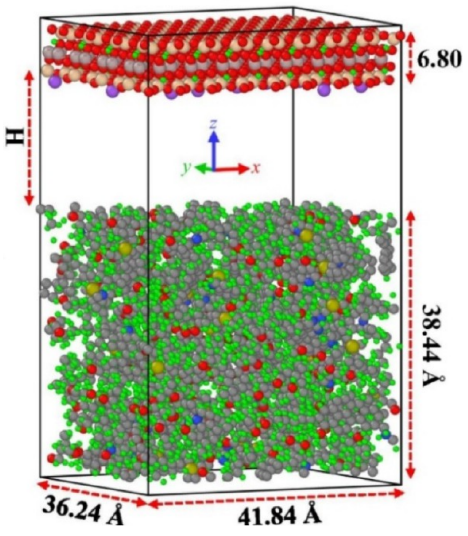

Figure 19. MMT−kerogen composite simulation models with lattice-related parameters. Reprinted from ref 107, Copyright 2022, with permission from Elsevier, 10.1016/j.molliq.2022.119263.

microscope field and an ion-milling device (i.e., FIB: focused ion beam) were added to the SEM/TEM in turn to obtain higher-resolution 2D images.[119] Chalmers et al. combined FIB-SEM and FIB-TEM to obtain high-resolution images (similar to 5 nm) of gas shale pore systems.[120]

The high resolution of SEM combined with the precise cutting capability of FIB allows direct 3D imaging with a

https://doi.org/10.1021/acsomega.3c01036
ACS Omega 2023, 8, 13519−13538

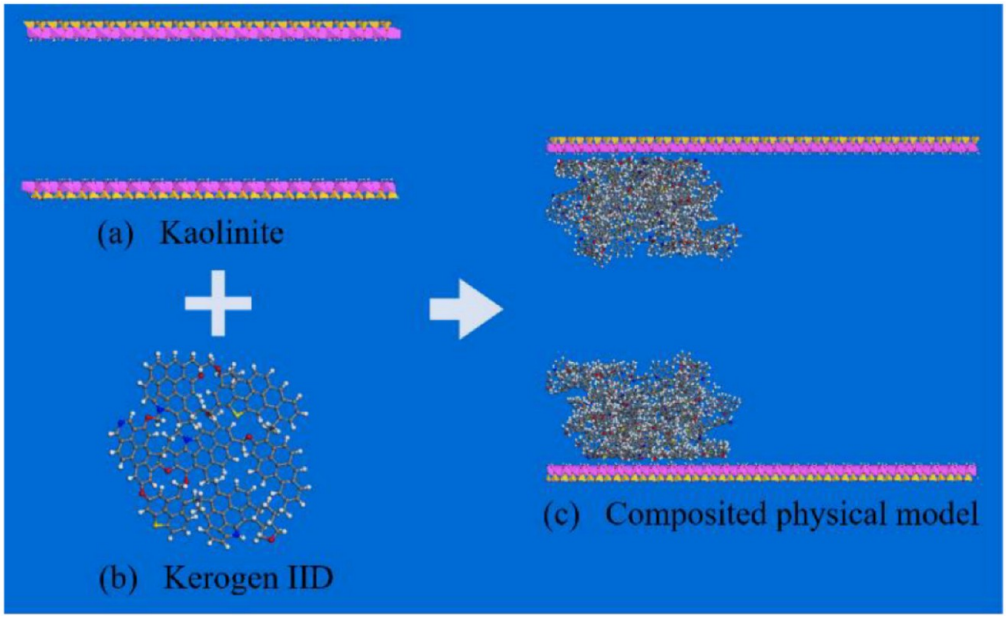

Figure 20. Composite shale model of kaolinite and kerogen II-D. Reproduced from ref 108, Copyright 2020, Multidisciplinary Digital Publishing Institute.

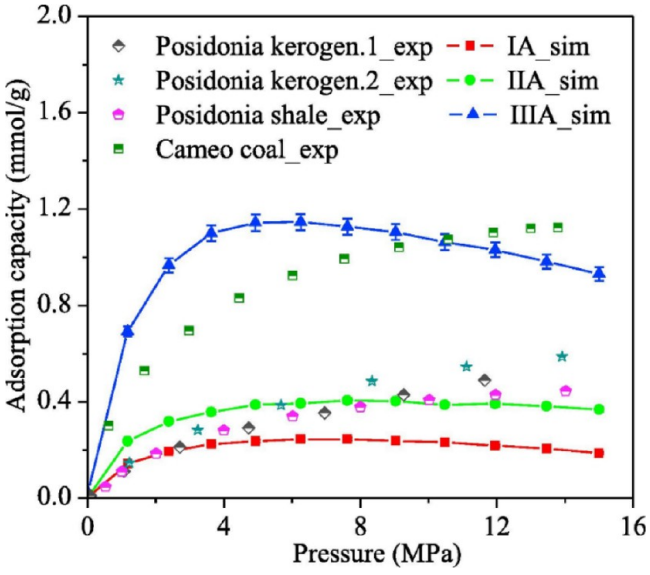

Figure 21. Comparison of CH_4 excess adsorption isotherms between simulated results and experimental data at 338 K. Reprinted from ref 72, Copyright 2017, with permission from Elsevier, 10.1016/j.apenergy.2017.10.122.

resolution of a few nanometers.[15] X-ray microtomography is also a common technique for imaging three-dimensional microstructures.[121] Pore size distribution and porosity can be calculated from the 3D digital models created by the above-mentioned techniques.[115] Zhou et al. reconstructed and segmented the three-dimensional digital cores of the Longmaxi Formation by means of FIB-SEM and calculated the average pore size of 32 nm and porosity of 3.62%.[15] Besides, image acquisition and analysis were performed using X-ray microtomography and FIB-SEM to set up 3D gradients and marker-based watershed transformations, segmenting and visualizing organic matter, minerals, and pore phases of oil shale samples from the Green River Formation.[121] In conclusion, even though FIB-SEM is expensive and time-consuming, which limits the number of samples analyzed, it is the most effective 2D and 3D imaging technique for characterizing shale nanopores, which is beneficial for shale gas reservoir exploration and development evaluation.

The advantages and disadvantages of direct imaging methods and their applicable occasions are listed in Table 2.

3.2. Indirect Methods. Indirect methods can estimate the bulk properties including porosity, pore size. and morphology and indicate the composition of shale samples.[14,116] In this section, common indirect measurement methods are described, such as helium porosity measurements, low-pressure N_2 gas adsorption (LP-N_2-GA), mercury intrusion capillary pressure (MICP), nuclear magnetic resonance (NMR), and X-ray diffraction (XRD).

3.2.1. Helium Porosity Measurement. Helium is an inert gas with a very small molecular diameter and is insensitive to any chemical reaction. Helium can penetrate pores with diameters on the order of micropores and has the lowest tendency to adsorb on pore surfaces, making the helium porosity measurement a very reliable shale porosity measurement technique.[122] Chakraborty et al. measured the porosity of the shale samples using helium, methane, and argon, respectively, and the results obtained from helium porosity measurements were between 5% and 16.4%, which is within the range of porosity for shales in general.[122] However, the porosity obtained using methane and argon was much higher than the normal porosity levels, which is apparently due to adsorption phenomena. The helium porosity measurement can also be used to compare particle density, bulk density, and total porosity of shale samples.[123,124] Li et al. investigated the effect of comminution of shale samples on shale pore characteristics by helium porosity measurements.[125] The results showed that comminution reduced the proportion of helium inaccessible pores and greatly increased the shale porosity. Therefore, the analytical shale particle size for helium porosity measurements is not recommended to be excessive; less than 20 mesh is a more appropriate range.[125] Overall, the porosity measured

https://doi.org/10.1021/acsomega.3c01036
ACS Omega 2023, 8, 13519−13538

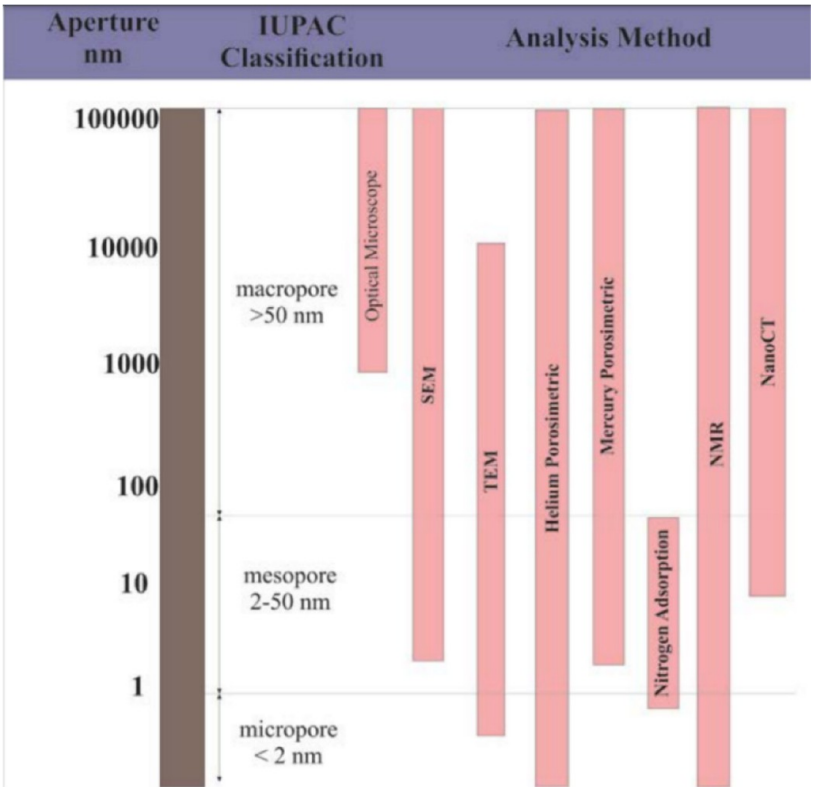

Figure 22. Various analytical methods/techniques used for estimating porosity and pore size distributions in unconventional gas reservoirs. Reproduced from ref 14, Copyright 2018, IOP Science.

Table 2. Comparison of Direct Imaging Methods

direct imaging methods	TEM	SEM	FIB-SEM
advantages	1. a relatively high resolution 2. clearly observing mesopores in the shale	1. relatively low cost 2. clearly observing fracture structure in the shale	1. enabling both 2D and 3D microstructure imaging 2. comprehensive representatives of pore structure 3. calculable pore size distribution and porosity
disadvantages	1. high cost 2. limited number of sample analyses 3. few representatives of pore structure	1. a relatively low resolution 2. few representatives of pore structure	1. extremely high cost 2. time consuming
applicable occasions	1. characterization of shale nanopores using 2D imaging		1. characterization of shale nanopores using 2D and 3D imaging

using helium, which has the smallest molecular diameter, is the most reflective of the effective porosity of the shale sample. However, due to the low permeability of the shale samples, it takes a relatively long time for helium to diffuse and equilibrate in the shale samples.

3.2.2. Low-Pressure Gas Adsorption. Low-pressure gas adsorption is a well-established method for characterizing pore structure, which has been applied to characterize the pore structure of shale samples in previous studies.[126−131] The pore size distribution is calculated using capillary condensation based on the Kelvin Equation in the pore through gas adsorption/desorption.[116] Nitrogen adsorption at 77 K is the standard method for analyzing pore sizes, which is highly accurate for mesopores and macropores in shale samples.[129] N_2 adsorption at 77 K can detect pores with diameters greater than or equal to 1.3 nm.[116] On the other hand, the specific interaction of nitrogen molecules with functional groups on the adsorption surface, which affects the micropore-filling pressure, leads to inaccurate detection of micropores.[132] The relatively high boiling point and high saturation vapor pressure of CO_2 make its adsorption at 273 K a promising method for studying narrow micropores (as small as 0.33 nm) in shale.[132] Thus, the combined CO_2 and N_2 adsorption data cover a range of pore sizes from micropores to macropores in shale nanopores, allowing information on the properties of shale porous structures, such as surface area and pore structure. Zou et al. quantified pores in shales with sizes ranging from 0.4 to 100 nm by low-pressure N_2 and CO_2 adsorption and further investigated the effect of moisture on the structure of shale samples.[131] In another example, low-pressure N_2 and CO_2 isotherms were used to construct the full range of pore size distribution in the Lower Cretaceous terrestrial Shahezi shale, where mesopores were observed to contribute the most to the pore volume, followed by macropores.[127] In conclusion, the combination of CO_2 and N_2 adsorption provides a more comprehensive measurement of the pore structure, which provides information on a variety of pore structure properties, such as surface area and pore size. However, the low gas pressure adsorption experiment is time-consuming; for example, the degassing time for general samples recommended

https://doi.org/10.1021/acsomega.3c01036
ACS Omega 2023, 8, 13519−13538

Table 3. Comparison of Indirect Measurement Methods

indirect methods	helium porosity measurement	low-pressure gas adsorption	MICP	NMR	XRD
advantages	1. high accuracy 2. nondestructive	1. accurate identification of mesopores (N_2) and micropores (CO_2)	1. simple operation 2. cheap	1. high accuracy 2. nondestructive 3. predicting molecular motion within pores	1. high accuracy 2. time-saving 3. cheap
disadvantages	1. relatively time-consuming	1. difficulty in covering the full-scale pore size using single-gas adsorption	1. limitations on pore size measurement	1. high cost and cumbersome operation	1. highly influenced by the degree of mineral crystallization
applicable occasions	1. shale porosity measurement	1. measurement of pore structure properties	1. shale porosity measurement	1. pore structure detection and molecular motion prediction within pores	1. characterization of inorganic mineral composition

by IUPAC is at least 6 h, and for some microporous samples even more than 12 h is required. Therefore, molecular simulations can be used instead of experiments to achieve time-saving results in the case in which an accurate model is available. For instance, the GCMC method was used to simulate helium adsorption of a kerogen matrix in order to calculate and validate the effective pore volume.[109]

3.2.3. Mercury Intrusion Capillary Pressure (MICP). MICP measurement is the standard method for characterizing pore throat size distributions in media from the micron to nanometer scale.[116] MICP measurement is performed on shale samples of a few cubic centimeters in size, measuring the volume of mercury and the pressure injected, to obtain pore throat profiles and pore volume measurements.[133] MICP measurement is accurate for pores larger than 3 nm because the maximum pressure (60.000 psi) of the MICP instrument allows mercury to enter pores up to 3 nm thick.[133] Wang and Zai revealed that the MICP curves for shale core plugs with high permeability are characterized by low repulsion pressure, small slope of mercury compression, and numerous mercury compression processes.[134] In another example, hysteresis was observed in the MICP intrusion−extrusion curves for all three shale samples, indicating that more than 50% of the intruded mercury remained inside the samples after extrusion.[135] Furthermore, MICP and gas adsorption methods can be used in conjunction to characterize the pore structure of shale in the complete pore size range.[136] MICP is an affordable way to gain initial insight into the porosity of shale gas reservoirs without the need for unique and time-consuming processing methods. However, the limitation of the pore size that can be measured by MICP requires it to be used in combination with other techniques such as NMR.

3.2.4. Nuclear Magnetic Resonance (NMR). NMR is a powerful technique that can probe the state of molecular motion within pores and the structure of shale pores. The principle of NMR is to obtain information on pore space (size, shape, and volume) by quantifying the interaction of protons and porous media.[137] In NMR measurements of shale, the parameter of transverse relaxation time (T_2) is widely used due to its fast speed, nondestructive detection, and rich information on core fluid. The T_2 distribution actually reflects the distribution of pore size, and the relationship between T_2 and pore size is positively correlated.[138] Huang and Zhao measured shale pore size distribution using NMR measurements and found that pore size varies over a multiscale range, with nanoscale pore volumes accounting for the majority.[137] Yuan et al. used NMR techniques to redefine the critical dehydration temperature in the Permian Carynginia shale and to determine the NMR T_2 cutoff for clay-bound water.[139] The NMR porosity of shales is usually lower than the density porosity, and the porosity difference increases with increasing TOC content, which makes the NMR measurement applicable in clay-rich shales.[140] Besides, the results of NMR and MICP measurements are integrated as complete data in some research due to the fact that NMR can characterize pores that cannot be characterized by MICP.[116] Recently, the NMR technique has gained great popularity owing to its capability not only to probe the pore structure but also to predict the molecular motion within the pores, despite its high price and cumbersome operation.

3.2.5. X-ray Diffraction (XRD). XRD is an effective technique for analyzing the mineral composition of shales by X-ray diffraction patterns.[141] Hui et al. investigated the effect of supercritical carbon dioxide ($ScCO_2$) exposure on the content of inorganic minerals in shale samples by the XRD technique.[142] The results showed that the shale samples mainly contained quartz, feldspar, carbonate minerals (calcite, dolomite), and clay minerals, and no significant changes in mineral composition were observed after $ScCO_2$ exposure.[142,143] In another example, the XRD technique was used to analyze the changes in mineral composition of the shale before and after treatment with H_2O_2 solution.[144] It was found that the dissolution capacity of pyrite was the greatest with H_2O_2 treatment, followed by chlorite, illite, calcite, dolomite, and feldspar, while quartz was almost unaffected as it showed a mass change rate of only 0.035%. Overall, XRD, which has the advantages of high accuracy, time-savings, and cheapness, is preferred in the characterization of the inorganic mineral composition of shale.

The advantages and disadvantages of indirect measurement methods and their applicable occasions are listed in Table 3.

Experiments provide a somewhat objective representation of adsorption levels on real shales, as well as allowing a more comprehensive understanding of the pore structure. However, there must be errors in the experimental process; for example, the cores used in most of the adsorption experiments require to be ground, leading to the destruction of the pore structure, which causes errors in the adsorption capacity of the shale. Obviously, adsorption simulations can avoid data errors due to sample destruction and are free from safety issues in high-temperature and high-pressure experimental environments. In addition, molecular simulations are a time- and money-saving tool that eliminates the need for experiment preparation time and the cost of equipment and sample purchases. Nevertheless, the accuracy of model construction is still dependent on real shale characterization experiments. Simulations and experiments are two effective means of conducting research, both of which complement and validate each other.

https://doi.org/10.1021/acsomega.3c01036
ACS Omega 2023, 8, 13519−13538

4. CONCLUSION

In this paper, different molecular models of shales, including organic matter models and inorganic mineral models, are reviewed, and the analysis of gas adsorption simulations on these models is presented. These molecular models with partial properties of real shales offer the possibility to study the behaviors and mechanism of gas adsorption on shale organic matter and inorganic minerals. Furthermore, in order to estimate the true adsorption capacity of shale gas in shale, it is necessary to understand the characteristics of the pore structure. Therefore, the experimental characterization methods for shale microstructure analysis are reviewed. Ultimately, the following conclusions were summarized for the above review.

1. Simplified shale organic models, such as graphene, CNTs, and nanoporous materials, can partially represent the properties of shale organics, but the gas adsorption simulations performed on them differ significantly from the reality due to the absence of functional groups and other elements in the real shale.
2. Kerogen unit models based on elemental and functional group data of kerogen in real shales are the mainstream of current research. The shale reservoirs are represented by the kerogen matrix models in gas adsorption simulations, and the kerogen slit models represent the natural fractures in the real shale reservoirs, which cover the entire shale pore size system. The gas adsorption capacity on these models allows for estimation of shale gas storage or some guidance on the amount of CO_2 injection in CO_2-EGR projects.
3. The studies of the gas adsorption in inorganic mineral models have made significant progress. The establishment of shale models that can accurately describe the composition and structure of shale is essential to perform molecular simulations of shale gas adsorption. Thus, a composite shale model composed of kerogen and inorganic minerals is fundamental to future simulation research.
4. Among the direct imaging methods, FIB-SEM is currently the most effective 2D and 3D imaging technique for characterizing shale nanopores. The following indirect methods, such as helium porosity measurements, combined CO_2 and nitrogen adsorption, and the integrated NMR and MICP measurements, can cover a range of pore sizes from micropores to macropores in shale nanopores. XRD is an effective technique for analyzing the mineral composition of shales. To characterize complex shale pore systems, multiple experimental characterization methods need to be used in combination, which means the results of direct imaging methods and indirect measurement methods should be integrated.
5. There are still some aspects that have not been covered in detail among the previous studies. Practical applications require dynamic adsorption models that reflect the influence of temporal parameters. In addition, current adsorption models rarely consider the capillary condensation phenomenon in which shale gas is mainly stored in nanopores. Furthermore, experimental studies of supercritical gas adsorption on intact shale cores are scarce, and it requires correspondingly accurate supercritical adsorption models to reveal the mechanism of gas adsorption in shale.

AUTHOR INFORMATION

Corresponding Author

Dexiang Li − *School of Energy and Power Engineering, Shandong University, Jinan 250061, China;* orcid.org/0000-0002-6937-572X; Email: de-xiang.li@sdu.edu.cn

Authors

Yufan Zhang − *School of Energy and Power Engineering, Shandong University, Jinan 250061, China;* orcid.org/0000-0002-7055-9841

Gongming Xin − *School of Energy and Power Engineering, Shandong University, Jinan 250061, China;* orcid.org/0000-0003-3974-0391

Shaoran Ren − *School of Petroleum Engineering, China University of Petroleum (East China), Qingdao 266580, China;* orcid.org/0000-0002-0829-3704

Complete contact information is available at: https://pubs.acs.org/10.1021/acsomega.3c01036

Notes

The authors declare no competing financial interest.

ACKNOWLEDGMENTS

The authors would like to acknowledge the Shandong Natural Science Foundation (ZR2019BA004) for the financial support of this research and allowing this Review to be published.

REFERENCES

(1) Bellani, J.; Verma, H. K.; Khatri, D.; Makwana, D.; Shah, M. N. Shale gas: a step toward sustainable energy future. *Journal of Petroleum Exploration and Production Technology* **2021**, *11* (5), 2127−2141.

(2) Zou, C. N.; Yang, Z.; Tao, S. Z.; Yuan, X.; Zhu, R. K.; Hou, L. H.; Wu, S. T.; Sun, L.; Zhang, G. S.; Bai, B.; Wang, L.; Gao, X. H.; Pang, Z. L. Continuous hydrocarbon accumulation over a large area as a distinguishing characteristic of unconventional petroleum: The Ordos Basin, North-Central China. *Earth-Science Reviews* **2013**, *126*, 358−369.

(3) Chalmers, G. R. L.; Bustin, R. M. Lower Cretaceous gas shales in northeastern British Columbia, Part I: geological controls on methane sorption capacity. *Bulletin of Canadian Petroleum Geology* **2008**, *56* (1), 1−21.

(4) Mastalerz, M.; Drobniak, A.; Rupp, J. Meso- and Micropore Characteristics of Coal Lithotypes: Implications for CO_2 Adsorption. *Energy Fuels* **2008**, *22* (6), 4049−4061.

(5) Ross, D. J. K.; Bustin, R. M. Characterizing the shale gas resource potential of Devonian-Mississippian strata in the Western Canada sedimentary basin: Application of an integrated formation evaluation. *Aapg Bulletin* **2008**, *92* (1), 87−125.

(6) McGlade, C.; Speirs, J.; Sorrell, S. Unconventional gas - A review of regional and global resource estimates. *Energy* **2013**, *55*, 571−584.

(7) Li, J.; Wang, Y.; Chen, Z.; Rahman, S. S. Simulation of Adsorption−Desorption Behavior in Coal Seam Gas Reservoirs at the Molecular Level: A Comprehensive Review. *Energy Fuels* **2020**, *34* (3), 2619−2642.

(8) Sander, R.; Connell, L. D.; Pan, Z.; Camilleri, M.; Heryanto, D.; Lupton, N. Core flooding experiments of CO2 enhanced coalbed methane recovery. *International Journal of Coal Geology* **2014**, *131*, 113−125.

(9) Odoh, S. O.; Cramer, C. J.; Truhlar, D. G.; Gagliardi, L. Quantum-Chemical Characterization of the Properties and Reactivities of Metal-Organic Frameworks. *Chem. Rev.* **2015**, *115* (12), 6051−111.

https://doi.org/10.1021/acsomega.3c01036
ACS Omega 2023, 8, 13519−13538

(10) He, S.; Jiang, Y.; Conrad, J. C.; Qin, G. Molecular simulation of natural gas transport and storage in shale rocks with heterogeneous nano-pore structures. *J. Pet. Sci. Eng.* **2015**, *133*, 401−409.
(11) Wang, Z. H.; Li, Y.; Liu, H.; Zeng, F. H.; Guo, P.; Jiang, W. Study on the Adsorption, Diffusion and Permeation Selectivity of Shale Gas in Organics. *Energies* **2017**, *10* (1), 142.
(12) Gartner, T. E.; Jayaraman, A. Modeling and Simulations of Polymers: A Roadmap. *Macromolecules* **2019**, *52* (3), 755−786.
(13) Wang, H.; Qu, Z. G.; Yin, Y.; Bai, J. Q.; Yu, B. Review of Molecular Simulation Method for Gas Adsorption/desorption and Diffusion in Shale Matrix. *Journal of Thermal Science* **2019**, *28* (1), 1−16.
(14) Listiyowati, L. N. Laboratory characterization of shale pores. *IOP Conference Series: Earth and Environmental Science* **2018**, *118*, 012067.
(15) Zhou, S.; Yan, G.; Xue, H.; Guo, W.; Li, X. 2D and 3D nanopore characterization of gas shale in Longmaxi formation based on FIB-SEM. *Marine and Petroleum Geology* **2016**, *73*, 174−180.
(16) Zhu, H.; Huang, C.; Ju, Y.; Bu, H.; Li, X.; Yang, M.; Chu, Q.; Feng, H.; Qiao, P.; Qi, Y.; Ma, P.; Zheng, L.; Lu, Y. Multi-scale multi-dimensional characterization of clay-hosted pore networks of shale using FIBSEM, TEM, and X-ray micro-tomography: Implications for methane storage and migration. *Appl. Clay Sci.* **2021**, *213*, 106239.
(17) Wang, M.; Yu, Q. Pore structure characterization of Carboniferous shales from the eastern Qaidam Basin, China: Combining helium expansion with low-pressure adsorption and mercury intrusion. *J. Pet. Sci. Eng.* **2017**, *152*, 91−103.
(18) Guo, C.; Li, R.; Sun, J.; Wang, X.; Liu, H. A review of gas transport and adsorption mechanisms in two-component methane-carbon dioxide system. *International Journal of Energy Research* **2020**, *44* (4), 2499−2516.
(19) Liu, S.; Sun, B.; Xu, J.; Li, H.; Wang, X. Study on Competitive Adsorption and Displacing Properties of CO_2 Enhanced Shale Gas Recovery: Advances and Challenges. *Geofluids* **2020**, *2020*, 6657995.
(20) Liang, H.; Qi, Z.; Wang, S.; Huang, X.; Yan, W.; Yuan, Y.; Li, Z. Adsorption Models for Shale Gas: A Mini-Review. *Energy Fuels* **2022**, *36* (21), 12946−12960.
(21) Rani, S.; Padmanabhan, E.; Prusty, B. K. Review of gas adsorption in shales for enhanced methane recovery and CO_2 storage. *J. Pet. Sci. Eng.* **2019**, *175*, 634−643.
(22) Wang, H.; Qu, Z. G.; Yin, Y.; Bai, J. Q.; Yu, B. Review of Molecular Simulation Method for Gas Adsorption/desorption and Diffusion in Shale Matrix. *Journal of Thermal Science* **2019**, *28* (1), 1−16.
(23) Memon, A.; Memon, B. S.; Muther, T.; Qureshi, A. S.; Uqaili, U. A.; Jeswani, S. S.; Zardari, Z. H. Quantitative models and controlling factors of Langmuir volume and pressure for the measurement of shale gas adsorption: An Analytical study based review. *Arabian Journal of Geosciences* **2022**, *15*, 754.
(24) Wang, T.; Tian, S.; Li, G.; Zhang, L.; Sheng, M.; Ren, W. Molecular simulation of gas adsorption in shale nanopores: A critical review. *Renewable and Sustainable Energy Reviews* **2021**, *149*, 111391.
(25) Klewiah, I.; Berawala, D. S.; Alexander Walker, H. C.; Andersen, P. Ø.; Nadeau, P. H. Review of experimental sorption studies of CO_2 and CH_4 in shales. *Journal of Natural Gas Science and Engineering* **2020**, *73*, 103045.
(26) Du, F.; Nojabaei, B. A Review of Gas Injection in Shale Reservoirs: Enhanced Oil/Gas Recovery Approaches and Greenhouse Gas Control. *Energies* **2019**, *12* (12), 2355.
(27) Jeong, S. R.; Park, J. H.; Lee, J. H.; Jeon, P. R.; Lee, C.-H. Review of the adsorption equilibria of CO_2, CH_4, and their mixture on coals and shales at high pressures for enhanced CH_4 recovery and CO_2 sequestration. *Fluid Phase Equilib.* **2023**, *564*, 113591.
(28) Zhai, Z. Q.; Wang, X. Q.; Jin, X.; Sun, L.; Li, J. M.; Cao, D. P. Adsorption and Diffusion of Shale Gas Reservoirs in Modeled Clay Minerals at Different Geological Depths. *Energy Fuels* **2014**, *28* (12), 7467−7473.
(29) Wang, H.; Chen, L.; Qu, Z. G.; Yin, Y.; Kang, Q. J.; Yu, B.; Tao, W. Q. Modeling of multi-scale transport phenomena in shale gas production - A critical review. *Applied Energy* **2020**, *262*, 114575.
(30) Orendt, A. M.; Pimienta, I. S. O.; Badu, S. R.; Solum, M. S.; Pugmire, R. J.; Facelli, J. C.; Locke, D. R.; Chapman, K. W.; Chupas, P. J.; Winans, R. E. Three-Dimensional Structure of the Siskin Green River Oil Shale Kerogen Model: A Comparison between Calculated and Observed Properties. *Energy Fuels* **2013**, *27* (2), 702−710.
(31) Bousige, C.; Ghimbeu, C. M.; Vix-Guterl, C.; Pomerantz, A. E.; Suleimenova, A.; Vaughan, G.; Garbarino, G.; Feygenson, M.; Wildgruber, C.; Ulm, F. J.; Pellenq, R. J. M.; Coasne, B. Realistic molecular model of kerogen's nanostructure. *Nat. Mater.* **2016**, *15* (5), 576.
(32) Zhou, W. D.; Xie, S. Y.; Bao, Z. Y.; Carranza, E. J. M.; Wang, Y.; Tang, M. L. Modeling of the Correlation Between Mineral Size and Shale Pore Structure at Meso- and Macroscales. *Mathematical Geosciences* **2022**, *54* (1), 131−150.
(33) Li, G. Z.; Huang, B.; Pan, Z. F.; Su, X. Y.; Shao, Z. P.; An, L. Advances in three-dimensional graphene-based materials: configurations, preparation and application in secondary metal (Li, Na, K, Mg, Al)-ion batteries. *Energy Environ. Sci.* **2019**, *12* (7), 2030−2053.
(34) Chen, C.; Sun, J.; Zhang, Y.; Mu, J.; Li, W.; Song, Y. Adsorption characteristics of CH_4 and CO_2 in organic-inorganic slit pores. *Fuel* **2020**, *265*, 116969.
(35) Mosher, K.; He, J.; Liu, Y.; Rupp, E.; Wilcox, J. Molecular simulation of methane adsorption in micro- and mesoporous carbons with applications to coal and gas shale systems. *International Journal of Coal Geology* **2013**, *109−110*, 36−44.
(36) Sun, J.; Chen, C.; Zhang, Y.; Li, W.; Song, Y. Competitive adsorption characteristics based on partial pressure and adsorption mechanism of CO_2/CH_4 mixture in shale pores. *Chem. Eng. J.* **2022**, *430*, 133172.
(37) Cao, J.; Liang, Y.; Masuda, Y.; Koga, H.; Tanaka, H.; Tamura, K.; Takagi, S.; Matsuoka, T. Molecular simulation of CH_4 adsorption behavior in slit nanopores: Verification of simulation methods and models. *AIChE J.* **2019**, *65* (11), e16733.
(38) Pitakbunkate, T.; Balbuena, P. B.; Moridis, G. J.; Blasingame, T. A. Effect of Confinement on Pressure/Volume/Temperature Properties of Hydrocarbons in Shale Reservoirs. *Spe Journal* **2016**, *21* (2), 621−634.
(39) Xiong, J.; Liu, X.; Liang, L.; Zeng, Q. Adsorption of methane in organic-rich shale nanopores: An experimental and molecular simulation study. *Fuel* **2017**, *200*, 299−315.
(40) Li, Y.; Hu, Z.; Liu, X.; Gao, S.; Duan, X.; Chang, J.; Wu, J. Insights into interactions and microscopic behavior of shale gas in organic−rich nano−slits by molecular simulation. *Journal of Natural Gas Science and Engineering* **2018**, *59*, 309−325.
(41) Zhao, J. F.; Wang, Z. H.; Guo, P. Microscopic Simulation of Methane Adsorption in Organic Matter. *Ind. Eng. Chem. Res.* **2019**, *58* (8), 3523−3530.
(42) Liu, B.; Qi, C.; Mai, T.; Zhang, J.; Zhan, K.; Zhang, Z.; He, J. Competitive adsorption and diffusion of CH4/CO2 binary mixture within shale organic nanochannels. *Journal of Natural Gas Science and Engineering* **2018**, *53*, 329−336.
(43) Shi, K.; Chen, J.; Pang, X.; Jiang, F.; Hui, S.; Pang, H.; Ma, K.; Cong, Q. Effect of wettability of shale on CO_2 sequestration with enhanced gas recovery in shale reservoir: Implications from molecular dynamics simulation. *Journal of Natural Gas Science and Engineering* **2022**, *107*, 104798.
(44) Akbarzadeh, H.; Abbaspour, M.; Salemi, S.; Akbari, M. Injection of mixture of shale gases in a nanoscale pore of graphite and their displacement by CO_2/N_2 gases using molecular dynamics study. *J. Mol. Liq.* **2017**, *248*, 439−446.
(45) Naveen, P.; Asif, M.; Ojha, K.; Panigrahi, D. C.; Vuthaluru, H. B. Sorption Kinetics of CH_4 and CO_2 Diffusion in Coal: Theoretical and Experimental Study. *Energy Fuels* **2017**, *31* (7), 6825−6837.
(46) Ansari, R.; Ajori, S.; Ameri, A. Elastic and structural properties and buckling behavior of single-walled carbon nanotubes under

https://doi.org/10.1021/acsomega.3c01036
ACS Omega 2023, 8, 13519−13538

chemical adsorption of atomic oxygen and hydroxyl. *Chem. Phys. Lett.* **2014**, *616*, 120−125.
(47) Huang, L. L.; Zhang, L. Z.; Shao, Q.; Lu, L. H.; Lu, X. H.; Jiang, S. Y.; Shen, W. F. Simulations of binary mixture adsorption of carbon dioxide and methane in carbon nanotubes: Temperature, pressure, and pore size effects. *J. Phys. Chem. C* **2007**, *111* (32), 11912−11920.
(48) Lan, J. H.; Cheng, D. J.; Cao, D. P.; Wang, W. C. Silicon nanotube as a promising candidate for hydrogen storage: From the first principle calculations to grand canonical Monte Carlo simulations. *J. Phys. Chem. C* **2008**, *112* (14), 5598−5604.
(49) Kumar, K. V.; Muller, E. A.; Rodriguez-Reinoso, F. Effect of Pore Morphology on the Adsorption of Methane/Hydrogen Mixtures on Carbon Micropores. *J. Phys. Chem. C* **2012**, *116* (21), 11820−11829.
(50) Adisa, O. O.; Cox, B. J.; Hill, J. M. Modelling the surface adsorption of methane on carbon nanostructures. *Carbon* **2011**, *49* (10), 3212−3218.
(51) Zhu, X.; Zhao, Y.-P. Atomic Mechanisms and Equation of State of Methane Adsorption in Carbon Nanopores. *J. Phys. Chem. C* **2014**, *118* (31), 17737−17744.
(52) Ohba, T.; Kaneko, K.; Yudasaka, M.; Iijima, S.; Takase, A.; Kanoh, H. Cooperative Adsorption of Supercritical CH_4 in Single-Walled Carbon Nanohorns for Compensation of Nanopore Potential. *J. Phys. Chem. C* **2012**, *116* (41), 21870−21873.
(53) Cao, D. P.; Zhang, X. R.; Chen, J. F.; Wang, W. C.; Yun, J. Optimization of single-walled carbon nanotube arrays for methane storage at room temperature. *J. Phys. Chem. B* **2003**, *107* (48), 13286−13292.
(54) Wang, S.; Feng, Q. H.; Javadpour, F.; Zha, M.; Cui, R. H. Multiscale Modeling of Gas Transport in Shale Matrix: An Integrated Study of Molecular Dynamics and Rigid-Pore-Network Model. *Spe Journal* **2020**, *25* (3), 1416−1442.
(55) Yuan, Q.; Zhu, X.; Lin, K.; Zhao, Y. P. Molecular dynamics simulations of the enhanced recovery of confined methane with carbon dioxide. *Phys. Chem. Chem. Phys.* **2015**, *17* (47), 31887−93.
(56) Yeganegi, S.; Gholampour, F. Methane adsorption and diffusion in a model nanoporous carbon: an atomistic simulation study. *Adsorption* **2013**, *19* (5), 979−987.
(57) Lu, X.; Jin, D.; Wei, S.; Zhang, M.; Zhu, Q.; Shi, X.; Deng, Z.; Guo, W.; Shen, W. Competitive adsorption of a binary CO_2-CH_4 mixture in nanoporous carbons: effects of edge-functionalization. *Nanoscale* **2015**, *7* (3), 1002−12.
(58) Xiang, J. H.; Zeng, F. G.; Liang, H. Z.; Li, B.; Song, X. X. Molecular simulation of the $CH_4/CO_2/H_2O$ adsorption onto the molecular structure of coal. *Science China-Earth Sciences* **2014**, *57* (8), 1749−1759.
(59) Zhang, H.; Zeng, X.; Zhao, Z.; Zhai, Z.; Cao, D. Adsorption and selectivity of CH_4 /CO_2 in functional group rich organic shales. *Journal of Natural Gas Science and Engineering* **2017**, *39*, 82−89.
(60) Dang, Y.; Zhao, L. M.; Lu, X. Q.; Xu, J.; Sang, P. P.; Guo, S.; Zhu, H. Y.; Guo, W. Y. Molecular simulation of CO_2/CH_4 adsorption in brown coal: Effect of oxygen-, nitrogen-, and sulfur-containing functional groups. *Appl. Surf. Sci.* **2017**, *423*, 33−42.
(61) Ungerer, P.; Collell, J.; Yiannourakou, M. Molecular Modeling of the Volumetric and Thermodynamic Properties of Kerogen: Influence of Organic Type and Maturity. *Energy Fuels* **2015**, *29* (1), 91−105.
(62) Sui, H. G.; Yao, J. Effect of surface chemistry for CH_4/CO_2 adsorption in kerogen: A molecular simulation study. *Journal of Natural Gas Science and Engineering* **2016**, *31*, 738−746.
(63) Kelemen, S. R.; Afeworki, M.; Gorbaty, M. L.; Sansone, M.; Kwiatek, P. J.; Walters, C. C.; Freund, H.; Siskin, M.; Bence, A. E.; Curry, D. J.; Solum, M.; Pugmire, R. J.; Vandenbroucke, M.; Leblond, M.; Behar, F. Direct characterization of kerogen by x-ray and solid-state C-13 nuclear magnetic resonance methods. *Energy Fuels* **2007**, *21* (3), 1548−1561.
(64) Chong, L.; Sanguinito, S.; Goodman, A. L.; Myshakin, E. M. Molecular characterization of carbon dioxide, methane, and water adsorption in micropore space of kerogen matrix. *Fuel* **2021**, *283*, 119254.
(65) Collell, J.; Galliero, G.; Vermorel, R.; Ungerer, P.; Yiannourakou, M.; Montel, F.; Pujol, M. Transport of Multicomponent Hydrocarbon Mixtures in Shale Organic Matter by Molecular Simulations. *J. Phys. Chem. C* **2015**, *119* (39), 22587−22595.
(66) Pathak, M.; Huang, H.; Meakin, P.; Deo, M. Molecular investigation of the interactions of carbon dioxide and methane with kerogen: Application in enhanced shale gas recovery. *Journal of Natural Gas Science and Engineering* **2018**, *51*, 1−8.
(67) Song, R.; Cui, M. Molecular simulation on competitive adsorption mechanism of CH_4/CO_2 on shale kerogen. *Arabian Journal of Geosciences* **2018**, *11*, 403.
(68) Sun, H.; Zhao, H.; Qi, N.; Li, Y. Molecular Insights into the Enhanced Shale Gas Recovery by Carbon Dioxide in Kerogen Slit Nanopores. *J. Phys. Chem. C* **2017**, *121* (18), 10233−10241.
(69) Sun, Q.; Liu, W.; Zhang, N. Molecular insights into recovery of shale gas by CO_2 injection in kerogen slit nanopores. *Journal of Natural Gas Science and Engineering* **2021**, *90*, 103903.
(70) Wang, S.; Yao, X.; Feng, Q.; Javadpour, F.; Yang, Y.; Xue, Q.; Li, X. Molecular insights into carbon dioxide enhanced multi-component shale gas recovery and its sequestration in realistic kerogen. *Chem. Eng. J.* **2021**, *425*, 130292.
(71) Zhou, W.; Wang, H.; Yang, X.; Liu, X.; Yan, Y. Confinement Effects and CO2/CH4Competitive Adsorption in Realistic Shale Kerogen Nanopores. *Ind. Eng. Chem. Res.* **2020**, *59* (14), 6696−6706.
(72) Huang, L.; Ning, Z.; Wang, Q.; Zhang, W.; Cheng, Z.; Wu, X.; Qin, H. Effect of organic type and moisture on CO_2/CH_4 competitive adsorption in kerogen with implications for CO_2 sequestration and enhanced CH_4 recovery. *Applied Energy* **2018**, *210*, 28−43.
(73) Tesson, S.; Firoozabadi, A. Methane Adsorption and Self-Diffusion in Shale Kerogen and Slit Nanopores by Molecular Simulations. *J. Phys. Chem. C* **2018**, *122* (41), 23528−23542.
(74) Sun, Z.; Li, X.; Liu, W.; Zhang, T.; He, M.; Nasrabadi, H. Molecular dynamics of methane flow behavior through realistic organic nanopores under geologic shale condition: Pore size and kerogen types. *Chem. Eng. J.* **2020**, *398*, 124341.
(75) Rezlerova, E.; Brennan, J. K.; Lisal, M. Methane and carbon dioxide indual-porosityorganic matter: molecular simulations of adsorption and diffusion. *AIChE J.* **2021**, *67*, e16655.
(76) Michalec, L.; Lisal, M. Molecular simulation of shale gas adsorption onto overmature type II model kerogen with control microporosity. *Mol. Phys.* **2017**, *115* (9−12), 1086−1103.
(77) Huang, P.; Shen, L.; Maggi, F.; Chen, Z.; Pan, Z. Influence of surface roughness on methane flow in shale kerogen nano-slits. *Journal of Natural Gas Science and Engineering* **2022**, *103*, 104650.
(78) Liu, J.; Xie, H.; Wang, Q.; Chen, S.; Hu, Z. Influence of Pore Structure on Shale Gas Recovery with CO_2 Sequestration: Insight Into Molecular Mechanisms. *Energy Fuels* **2020**, *34* (2), 1240−1250.
(79) Zhou, W. N.; Zhang, Z.; Wang, H. B.; Yang, X. Molecular Investigation of CO_2/CH_4 Competitive Adsorption and Confinement in Realistic Shale Kerogen. *Nanomaterials* **2019**, *9* (12), 1646.
(80) Yang, C.; Zhang, J. C.; Han, S. B.; Wang, X. Z.; Wang, L.; Yu, W. W.; Wang, Z. G. Compositional controls on pore-size distribution by nitrogen adsorption technique in the Lower Permian Shanxi Shales, Ordos Basin. *Journal of Natural Gas Science and Engineering* **2016**, *34*, 1369−1381.
(81) Zhang, J. Z.; Li, X. Q.; Xie, Z. Y.; Li, J.; Zhang, X. Q.; Sun, K. X.; Wang, F. Y. Characterization of microscopic pore types and structures in marine shale: Examples from the Upper Permian Dalong formation, Northern Sichuan Basin, South China. *Journal of Natural Gas Science and Engineering* **2018**, *59*, 326−342.
(82) Ross, D. J. K.; Bustin, R. M. The importance of shale composition and pore structure upon gas storage potential of shale gas reservoirs. *Marine and Petroleum Geology* **2009**, *26* (6), 916−927.
(83) Hu, X.; Deng, H.; Lu, C.; Tian, Y.; Jin, Z. Characterization of CO_2/CH_4 Competitive Adsorption in Various Clay Minerals in

https://doi.org/10.1021/acsomega.3c01036
ACS Omega 2023, 8, 13519−13538

Relation to Shale Gas Recovery from Molecular Simulation. *Energy Fuels* **2019**, *33* (9), 8202−8214.
(84) Liu, Y.; Hou, J. Selective adsorption of CO_2/CH_4 mixture on clay-rich shale using molecular simulations. *Journal of CO2 Utilization* **2020**, *39*, 101143.
(85) Mu, Z.; Ning, Z.; Lyu, F.; Liu, B. Sorption of Deep Shale Gas on Minerals and Organic Matter from Molecular Simulation. *Energy Fuels* **2023**, *37* (1), 251−259.
(86) Xiong, J.; Liu, K.; Liu, X.; Liang, L.; Zeng, Q. Molecular simulation of methane adsorption in slit-like quartz pores. *RSC Adv.* **2016**, *6* (112), 110808−110819.
(87) Yang, X.; Chen, Z.; Liu, X.; Xue, Z.; Yue, F.; Wen, J.; Li, M.; Xue, Y. Correction of gas adsorption capacity in quartz nanoslit and its application in recovering shale gas resources by CO_2 injection: A molecular simulation. *Energy* **2022**, *240*, 122789.
(88) Ji, L. M.; Zhang, T. W.; Milliken, K. L.; Qu, J. L.; Zhang, X. L. Experimental investigation of main controls to methane adsorption in clay-rich rocks. *Appl. Geochem.* **2012**, *27* (12), 2533−2545.
(89) Chang, F. R. C.; Skipper, N. T.; Sposito, G. COMPUTER-SIMULATION OF INTERLAYER MOLECULAR-STRUCTURE IN SODIUM MONTMORILLONITE HYDRATES. *Langmuir* **1995**, *11* (7), 2734−2741.
(90) Sun, H.; Zhao, H.; Qi, N.; Qi, X.; Zhang, K.; Li, Y. Molecular insight into the micro-behaviors of CH4 and CO2 in montmorillonite slit-nanopores. *Mol. Simul.* **2017**, *43* (13−16), 1004−1011.
(91) Zhang, H.; Cao, D. Molecular simulation of displacement of shale gas by carbon dioxide at different geological depths. *Chem. Eng. Sci.* **2016**, *156*, 121−127.
(92) Wang, S.; Feng, Q.; Javadpour, F.; Hu, Q.; Wu, K. Competitive adsorption of methane and ethane in montmorillonite nanopores of shale at supercritical conditions: A grand canonical Monte Carlo simulation study. *Chem. Eng. J.* **2019**, *355*, 76−90.
(93) Chen, S. B.; Han, Y. F.; Fu, C. Q.; Zhang, H.; Zhu, Y. M.; Zuo, Z. X. Micro and nano-size pores of clay minerals in shale reservoirs: Implication for the accumulation of shale gas. *Sedimentary Geology* **2016**, *342*, 180−190.
(94) Szczerba, M.; Derkowski, A.; Kalinichev, A. G.; Srodon, J. Molecular modeling of the effects of 40Ar recoil in Illite particles on their K-Ar isotope dating. *Geochim. Cosmochim. Acta* **2015**, *159*, 162−176.
(95) Chen, G.; Lu, S.; Liu, K.; Han, T.; Xu, C.; Xue, Q.; Shen, B.; Guo, Z. GCMC simulations on the adsorption mechanisms of CH4 and CO2 in K-Illite and their implications for shale gas exploration and development. *Fuel* **2018**, *224*, 521−528.
(96) White, G. N.; Zelazny, L. W. ANALYSIS AND IMPLICATIONS OF THE EDGE STRUCTURE OF DIOCTAHEDRAL PHYLLOSILICATES. *Clays and Clay Minerals* **1988**, *36* (2), 141−146.
(97) Hao, Y.; Yuan, L.; Li, P.; Zhao, W.; Li, D.; Lu, D. Molecular Simulations of Methane Adsorption Behavior in Illite Nanopores Considering Basal and Edge Surfaces. *Energy Fuels* **2018**, *32* (4), 4783−4796.
(98) Warne, M. R.; Allan, N. L.; Cosgrove, T. Computer simulation of water molecules at kaolinite and silica surfaces. *Phys. Chem. Chem. Phys.* **2000**, *2* (16), 3663−3668.
(99) Zhou, W.; Wang, H.; Yan, Y.; Liu, X. Adsorption Mechanism of CO_2/CH_4 in Kaolinite Clay: Insight from Molecular Simulation. *Energy Fuels* **2019**, *33* (7), 6542−6551.
(100) Zhang, B.; Kang, J.; Kang, T. Effect of water on methane adsorption on the kaolinite (0 0 1) surface based on molecular simulations. *Appl. Surf. Sci.* **2018**, *439*, 792−800.
(101) Zhang, B.; Kang, J.; Kang, T.; Kang, G.; Zhao, G. Molecular dynamics simulations of CH_4 diffusion in kaolinite: influence of water content. *International Journal of Coal Science & Technology* **2019**, *6* (4), 556−563.
(102) Wang, K.; Zhang, B.; Kang, T. The Effect of Mg, Fe(II), and Al Doping on CH(4): Adsorption and Diffusion on the Surface of Na-Kaolinite (001) by Molecular Simulations. *Molecules* **2020**, *25* (4), 1001.
(103) Carchini, G.; Hussein, I.; Al-Marri, M. J.; Shawabkeh, R.; Mahmoud, M.; Aparicio, S. A theoretical study of gas adsorption on α-quartz (0 0 1) for CO_2 enhanced natural gas recovery. *Appl. Surf. Sci.* **2020**, *525*, 146472.
(104) Sun, H.; Sun, W.; Zhao, H.; Sun, Y.; Zhang, D.; Qi, X.; Li, Y. Adsorption properties of CH4 and CO2 in quartz nanopores studied by molecular simulation. *RSC Adv.* **2016**, *6* (39), 32770−32778.
(105) Huang, L.; Zhou, W.; Xu, H.; Wang, L.; Zou, J.; Zhou, Q. Dynamic fluid states in organic-inorganic nanocomposite: Implications for shale gas recovery and CO_2 sequestration. *Chem. Eng. J.* **2021**, *411*, 128423.
(106) Lee, T.; Bocquet, L.; Coasne, B. Activated desorption at heterogeneous interfaces and long-time kinetics of hydrocarbon recovery from nanoporous media. *Nat. Commun.* **2016**, *7*, 11890.
(107) Lyu, F.; Ning, Z.; Yang, S.; Mu, Z.; Cheng, Z.; Wang, Z.; Liu, B. Molecular insights into supercritical methane sorption and self-diffusion in monospecific and composite nanopores of deep shale. *J. Mol. Liq.* **2022**, *359*, 119263.
(108) Gong, L.; Zhang, Y.; Li, N.; Gu, Z.-K.; Ding, B.; Zhu, C.-Y. Molecular Investigation on the Displacement Characteristics of CH_4 by CO_2, N_2 and Their Mixture in a Composite Shale Model. *Energies* **2021**, *14* (1), 2.
(109) Zhou, J.; Mao, Q.; Luo, K. H. Effects of Moisture and Salinity on Methane Adsorption in Kerogen: A Molecular Simulation Study. *Energy Fuels* **2019**, *33* (6), 5368−5376.
(110) Ekundayo, J. M.; Rezaee, R. Numerical Simulation of Gas Production from Gas Shale Reservoirs-Influence of Gas Sorption Hysteresis. *Energies* **2019**, *12* (18), 3405.
(111) Zhang, L. J.; Li, D. L.; Li, L.; Lu, D. T. Development of a new compositional model with multi-component sorption isotherm and slip flow in tight gas reservoirs. *Journal of Natural Gas Science and Engineering* **2014**, *21*, 1061−1072.
(112) Li, J.; Wu, Q. Z.; Jin, W. J.; Lu, J.; Nan, Z. Y. Logging evaluation of free-gas saturation and volume content in Wufeng-Longmaxi organic-rich shales in the Upper Yangtze Platform, China. *Marine and Petroleum Geology* **2019**, *100*, 530−539.
(113) Loucks, R. G.; Reed, R. M.; Ruppel, S. C.; Hammes, U. Spectrum of pore types and networks in mudrocks and a descriptive classification for matrix-related mudrock pores. *Aapg Bulletin* **2012**, *96* (6), 1071−1098.
(114) Loucks, R. G.; Reed, R. M.; Ruppel, S. C.; Jarvie, D. M. MORPHOLOGY, GENESIS, AND DISTRIBUTION OF NANO-METER-SCALE PORES IN SILICEOUS MUDSTONES OF THE MISSISSIPPIAN BARNETT SHALE. *Journal of Sedimentary Research* **2009**, *79* (11−12), 848−861.
(115) Dong, T.; Harris, N. B.; Ayranci, K.; Twemlow, C. E.; Nassichuk, B. R. Porosity characteristics of the Devonian Horn River shale, Canada: Insights from lithofacies classification and shale composition. *International Journal of Coal Geology* **2015**, *141−142*, 74−90.
(116) Josh, M.; Esteban, L.; Delle Piane, C.; Sarout, J.; Dewhurst, D. N.; Clennell, M. B. Laboratory characterisation of shale properties. *J. Pet. Sci. Eng.* **2012**, *88−89*, 107−124.
(117) Milliken, K. L.; Rudnicki, M.; Awwiller, D. N.; Zhang, T. Organic matter-hosted pore system, Marcellus Formation (Devonian), Pennsylvania. *AAPG Bulletin* **2013**, *97* (2), 177−200.
(118) Tripathy, A.; Kumar, A.; Srinivasan, V.; Singh, K. H.; Singh, T. N. Fractal analysis and spatial disposition of porosity in major indian gas shales using low-pressure nitrogen adsorption and advanced image segmentation. *Journal of Natural Gas Science and Engineering* **2019**, *72*, 103009.
(119) Tang, X.; Li, Q. L.; Zhang, B.; Wang, P.; Gu, L. X.; Ling, X. X.; Fei, C. H.; Li, J. H. The Chemical State and Occupancy of Radiogenic Pb, and Crystallinity of RW-1 Monazite Revealed by XPS and TEM. *Minerals* **2020**, *10* (6), 504.
(120) Chalmers, G. R.; Bustin, R. M.; Power, I. M. Characterization of gas shale pore systems by porosimetry, pycnometry, surface area, and field emission scanning electron microscopy/transmission electron microscopy image analyses: Examples from the Barnett,

https://doi.org/10.1021/acsomega.3c01036
ACS Omega 2023, 8, 13519−13538

Woodford, Haynesville, Marcellus, and Doig units. *Aapg Bulletin* **2012**, *96* (6), 1099−1119.
(121) Saif, T.; Lin, Q.; Butcher, A. R.; Bijeljic, B.; Blunt, M. J. Multi-scale multi-dimensional microstructure imaging of oil shale pyrolysis using X-ray micro-tomography, automated ultra-high resolution SEM. *MAPS Mineralogy and FIB-SEM. Applied Energy* **2017**, *202*, 628−647.
(122) Chakraborty, N.; Karpyn, Z.; Liu, S.; Yoon, H.; Dewers, T. Experimental evidence of gas densification and enhanced storage in nanoporous shales. *Journal of Natural Gas Science and Engineering* **2020**, *76*, 103120.
(123) Guo, S.; Lü, X.; Song, X.; Liu, Y. Methane adsorption characteristics and influence factors of Mesozoic shales in the Kuqa Depression, Tarim Basin, China. *J. Pet. Sci. Eng.* **2017**, *157*, 187−195.
(124) Song, L.; Martin, K.; Carr, T. R.; Ghahfarokhi, P. K. Porosity and storage capacity of Middle Devonian shale: A function of thermal maturity, total organic carbon, and clay content. *Fuel* **2019**, *241*, 1036−1044.
(125) Li, J.; Zhou, S.; Fu, D.; Li, Y.; Ma, Y.; Yang, Y.; Li, C. Changes in the pore characteristics of shale during comminution. *Energy Exploration & Exploitation* **2016**, *34* (5), 676−688.
(126) Chandra, D.; Vishal, V. A Comparative Analysis of Pore Attributes of Sub-Bituminous Gondwana Coal from the Damodar and Wardha Valleys: Implication for Enhanced Coalbed Methane Recovery. *Energy Fuels* **2022**, *36* (12), 6187−6197.
(127) Gao, F.; Song, Y.; Li, Z.; Xiong, F.; Chen, L.; Zhang, Y.; Liang, Z.; Zhang, X.; Chen, Z.; Joachim, M. Lithofacies and reservoir characteristics of the Lower Cretaceous continental Shahezi Shale in the Changling Fault Depression of Songliao Basin, NE China. *Marine and Petroleum Geology* **2018**, *98*, 401−421.
(128) Hazra, B.; Wood, D. A.; Vishal, V.; Varma, A. K.; Sakha, D.; Singh, A. K. Porosity controls and fractal disposition of organic-rich Permian shales using low-pressure adsorption techniques. *Fuel* **2018**, *220*, 837−848.
(129) Wei, M.; Zhang, L.; Xiong, Y.; Li, J.; Peng, P. a. Nanopore structure characterization for organic-rich shale using the non-local-density functional theory by a combination of N_2 and CO_2 adsorption. *Microporous Mesoporous Mater.* **2016**, *227*, 88−94.
(130) Yu, W.; Tang, H. Experimental study on the existence of nano-scale pores and the evolution of organic matter in organic-rich shale. *Nanotechnol. Rev.* **2019**, *8* (1), 156−167.
(131) Zou, J.; Rezaee, R.; Xie, Q.; You, L.; Liu, K.; Saeedi, A. Investigation of moisture effect on methane adsorption capacity of shale samples. *Fuel* **2018**, *232*, 323−332.
(132) Thommes, M.; Kaneko, K.; Neimark, A. V.; Olivier, J. P.; Rodriguez-Reinoso, F.; Rouquerol, J.; Sing, K. S. W. Physisorption of gases, with special reference to the evaluation of surface area and pore size distribution (IUPAC Technical Report). *Pure Appl. Chem.* **2015**, *87* (9−10), 1051−1069.
(133) Sigal, R. F. Mercury Capillary Pressure Measurements on Barnett Core. *Spe Reservoir Evaluation & Engineering* **2013**, *16* (4), 432−442.
(134) Wang, F.; Zai, Y. Fractal and multifractal characteristics of shale nanopores. *Results in Physics* **2021**, *25*, 104277.
(135) Wang, C.; Zhang, B.; Hu, Q.; Shu, Z.; Sun, M.; Bao, H. Laminae characteristics and influence on shale gas reservoir quality of lower Silurian Longmaxi Formation in the Jiaoshiba area of the Sichuan Basin, China. *Marine and Petroleum Geology* **2019**, *109*, 839−851.
(136) Yu, Y.; Luo, X.; Wang, Z.; Cheng, M.; Lei, Y.; Zhang, L.; Yin, J. A new correction method for mercury injection capillary pressure (MICP) to characterize the pore structure of shale. *Journal of Natural Gas Science and Engineering* **2019**, *68*, 102896.
(137) Huang, X.; Zhao, Y.-P. Characterization of pore structure, gas adsorption, and spontaneous imbibition in shale gas reservoirs. *J. Pet. Sci. Eng.* **2017**, *159*, 197−204.
(138) Hun, L.; Bing, Y.; Xixiang, S.; Xinyi, S.; Lifei, D. Fracturing fluid retention in shale gas reservoir from the perspective of pore size based on nuclear magnetic resonance. *Journal of Hydrology* **2021**, *601*, 126590.
(139) Yuan, Y.; Rezaee, R.; Verrall, M.; Hu, S.-Y.; Zou, J.; Testmanti, N. Pore characterization and clay bound water assessment in shale with a combination of NMR and low-pressure nitrogen gas adsorption. *International Journal of Coal Geology* **2018**, *194*, 11−21.
(140) Tan, M.; Mao, K.; Song, X.; Yang, X.; Xu, J. NMR petrophysical interpretation method of gas shale based on core NMR experiment. *J. Pet. Sci. Eng.* **2015**, *136*, 100−111.
(141) Liu, Z.; Gao, B.; Zhang, Y.; Du, W.; Feng, D.; Nie, H. Types and distribution of the shale sedimentary facies of the Lower Cambrian in Upper Yangtze area, South China. *Petroleum Exploration and Development* **2017**, *44* (1), 20−31.
(142) Hui, D.; Pan, Y.; Luo, P.; Zhang, Y.; Sun, L.; Lin, C. Effect of supercritical CO_2 exposure on the high-pressure CO_2 adsorption performance of shales. *Fuel* **2019**, *247*, 57−66.
(143) Yin, H.; Zhou, J.; Xian, X.; Jiang, Y.; Lu, Z.; Tan, J.; Liu, G. Experimental study of the effects of sub- and super-critical CO_2 saturation on the mechanical characteristics of organic-rich shales. *Energy* **2017**, *132*, 84−95.
(144) Bai, J.; Kang, Y.; Chen, M.; Chen, Z.; You, L.; Li, X.; Chen, G. Impact of surface chemistry and pore structure on water vapor adsorption behavior in gas shale. *Chem. Eng. J.* **2020**, *402*, 126238.

https://doi.org/10.1021/acsomega.3c01036
ACS Omega 2023, 8, 13519−13538